

## Article

# In Silico Identification of Tripeptides as Lead Compounds for the Design of KOR Ligands

Azzurra Stefanucci <sup>1</sup>, Valeria Iobbi <sup>2</sup>, Alice Della Valle <sup>1</sup>, Giuseppe Scioli <sup>1</sup>, Stefano Pieretti <sup>3</sup> , Paola Minosi <sup>3</sup>, Sako Mirzaie <sup>4</sup>, Ettore Novellino <sup>5</sup> and Adriano Mollica <sup>1,\*</sup> 

<sup>1</sup> Department of Pharmacy, University G. d'Annunzio Chieti, Via dei Vestini 31, 66100 Chieti, Italy; a.stefanucci@unich.it (A.S.); alice.dellavalle@unich.it (A.D.V.); giuseppe.scioli@unich.it (G.S.)

<sup>2</sup> Department of Pharmacy (DIFAR), University of Genova, 16128 Genova, Italy; valeria.iobbi@edu.unige.it

<sup>3</sup> Centro Nazionale Ricerca e Valutazione Preclinica e Clinica dei Farmaci, Istituto Superiore di Sanità, Viale Regina Elena 299, 00161 Rome, Italy; stefano.pieretti@iss.it (S.P.); paola.minosi@uniroma1.it (P.M.)

<sup>4</sup> Advanced Pharmaceutics and Drug Delivery Laboratory, Leslie L. Dan Faculty of Pharmacy, University of Toronto, 27 King's College Circle, Toronto, ON M5S 1A1, Canada; sako.biochem@gmail.com

<sup>5</sup> NGN Healthcare, Via Nazionale Torrette, 207, 83013 Mercogliano, Italy; etторе.novellino@unina.it

\* Correspondence: a.mollica@unich.it

**Abstract:** The kappa opioid receptor (KOR) represents an attractive target for the development of drugs as potential antidepressants, anxiolytics and analgesics. A robust computational approach may guarantee a reduction in costs in the initial stages of drug discovery, novelty and accurate results. In this work, a virtual screening workflow of a library consisting of ~6 million molecules was set up, with the aim to find potential lead compounds that could manifest activity on the KOR. This in silico study provides a significant contribution in the identification of compounds capable of interacting with a specific molecular target. The main computational techniques adopted in this experimental work include: (i) virtual screening; (ii) drug design and leads optimization; (iii) molecular dynamics. The best hits are tripeptides prepared via solution phase peptide synthesis. These were tested in vivo, revealing a good antinociceptive effect after subcutaneous administration. However, further work is due to delineate their full *pharmacological* profile, in order to verify the features predicted by the in silico outcomes.

**Keywords:** peptides; molecular modelling; k-opioid receptor; antinociceptive effect; binding



**Citation:** Stefanucci, A.; Iobbi, V.; Della Valle, A.; Scioli, G.; Pieretti, S.; Minosi, P.; Mirzaie, S.; Novellino, E.; Mollica, A. In Silico Identification of Tripeptides as Lead Compounds for the Design of KOR Ligands. *Molecules* **2021**, *26*, 4767. <https://doi.org/10.3390/molecules26164767>

Academic Editor: Carlotta Granchi

Received: 21 July 2021

Accepted: 4 August 2021

Published: 6 August 2021

**Publisher's Note:** MDPI stays neutral with regard to jurisdictional claims in published maps and institutional affiliations.



**Copyright:** © 2021 by the authors. Licensee MDPI, Basel, Switzerland. This article is an open access article distributed under the terms and conditions of the Creative Commons Attribution (CC BY) license (<https://creativecommons.org/licenses/by/4.0/>).

## 1. Introduction

Opioids represent the most effective and widely used analgesics to treat acute and intense pain since ancient times. Most of them are selective agonists of G-coupled opioid receptors  $\mu$ -,  $\delta$ -, and k-opioid receptors (MOR, DOR and KOR respectively) [1]. Although opioid receptors are the best-known therapeutic targets for the treatment of acute and chronic diseases, their clinical use is limited by adverse side effects such as tolerance and dependence; thus, the development of analgesics with reduced side effects and lack of tolerance remains a main target in the field of medicinal chemistry [2]. KORs are considered an attractive target for the discovery of safe analgesics avoiding side effects including respiratory depression, tolerance, dependence, and constipation. They are widely expressed throughout the central and peripheral nervous system; among them dinorphins (encoded by the Pdyn gene) primarily activate the KORs with very low affinity for MOR and DOR [3]. In contrast to MOR and DOR receptor agonists, KOR agonists have been recognized as analgesics without addiction and tolerance insurgence, despite their tendency to induce dysphoria, anhedonia and hallucinations [4,5]. The crystal structure of human KOR in complex with the selective antagonist JDTC has been resolved in 2012 [6]. Che et al. provided the crystal structure of human KOR in complex with the agonist MP1104 in the active-state [7,8]. These clarify the conformational differences between inactive and active states,

providing details on ligand–receptor interactions [7–10]. The activation of KOR by endogenous peptide or exogenous synthetic agonists is associated with behavioral and mood effects, including analgesia, sedation, and perceptual distortions [11–13], while antagonists binding at the same site block the activation of KOR; thus, they may be used for treatment of depression, anxiety, addictive disorders, and other psychiatric conditions [14,15].

KOR is the main subtype of opioid receptors responsible for mediating dynorphin-related actions and dynorphin-related peptides, such as stress, addiction, emotion, and perception. KOR agonists have also been shown to inhibit hyperalgesia induced by the  $\mu$  agonist receptor [9,16]. Recent studies have uncovered further potential therapeutic areas for KOR ligands, such as affective disorders and addiction-related behaviors. As recently demonstrated for other GPCRs, structural insights from active and inactive receptors can be exploited in virtual ligand screening protocols providing new compounds as promising analgesics [17,18]. Several groups have shown that, unlike other opioid receptors, KOR agonists inhibit dopamine efflux in the mesolimbic system and block the gratifying effects of abuse drugs such as heroin and cocaine [19–21]. Most KOR agonists belong to five chemical classes: endogenous peptides (dynorphins), benzodiazepines (diazepam, tipladom), benzazocines (bremazocine, pentazocine), arilacetamides (enadoline, U50488), and diterpenes (salvinorin A). Benzazocines, such as bremazocine, are not strictly selective KOR agonists, but they show strong analgesic effects. However, these molecules were discarded during clinical development due to psychotomimetic and dysphoric effects, although they had low tolerance potential and drug dependence [22,23]. KOR agonists were generally thought to exhibit adverse effects due to off-target action; thus, new  $\kappa$ -selective agonists such as aryl-acetamide derivatives (enadolines, U69593, U50488) were developed to avoid psychotomimetic and dysphoric effects; however, they also produce hallucinations and aversion [24,25].

Salvinorin A, a very potent and selective KOR agonist is known for its psychedelic effects [26]. Despite such a different chemical structure,  $\kappa$  receptor agonists have more or less psychotomimetic effects, and, therefore, clinical development has failed. Not surprisingly, the simultaneous inhibition of multiple neurotransmitter systems by KOR agonists causes complex multidimensional effects, such as hallucination, dysphoria and analgesia [27].

In addition, agonists induce phosphorylation of protein kinase 3 (GRK3) receptors of the  $\kappa$  receptor in the C-terminal region and the subsequent recruitment of  $\beta$ -arrestins, which are scaffolding proteins leading to the phosphorylation of P38 MAPK [28,29]. The identification of G proteins not dependent from the activation of P38 MAPK in the serotonergic neurons of the dorsal Rafe by the KOR agonist U50488 was a step forward into the elucidation of the mechanisms by which the receptor  $\kappa$  averages adverse effects. Interference on this signaling pathway in mice through receptor mutation (KORS369A), the deletion of GRK3 or the conditional cancellation of P38-MAPK blocks the adverse effects of  $\kappa$  agonists without reducing their analgesic effects [30–33]. These studies have important therapeutic implications because a selective partial  $\kappa$  receptor agonist that does not efficiently activate arrestin-dependent reporting could produce analgesia without significant dysphoria. In addition, the  $\kappa$ -receptor-mediated activation of the P38 MAPK in glia seems to be important for the development of hyperalgesia following peripheral neuropathy [34–36].

Roth and colleagues performed systematic pharmacological studies to discover a partial G receptor agonist, RB-64 (22-thiocyanatosalvinorin A) [26]. This study, using KO wild type and  $\beta$ -arrestin-2 mice, showed that RB-64-mediated G protein signaling induces analgesia and aversion, while  $\beta$ -arrestin-2 signaling averages sedation, anhedonia, and motor incoordination. This is a clear example of how the characterization of signaling pathways, which mediate specific behaviors, can ultimately be used for drug development. So far, almost all studies to determine the biased agonism of GPCR have investigated the partiality of a ligand for both protein G and  $\beta$ -arrestin, dependent only on downstream signaling.

Thus, diverse signals (e.g., phosphorylation of the PKC or GRK-dependent receptor) are a prerequisite. Over the years, several opioid ligands have been identified with the

deconvolution of mixture-based combinatorial libraries at the Torrey Pines Institute of Molecular Studies (TPIMS) [37,38]. Computational studies through molecular scaffolds, molecular properties, and structural fingerprints show the diversity of these libraries and their uniqueness, based on: (a) the partial overlap with the structural space of drugs; (b) the presence of scaffolds not contained in other collections of compounds; (c) the increased molecular complexity compared to libraries of compounds commonly used in high-throughput screening (HTS) programs [39]. Structure-based drug design employs methods of receptor-based virtual screening (VS) and molecular docking for binding pose prediction, hit identification, and lead optimization. As part of our ongoing effort to discover new  $\kappa$  modulators with novel structures [40], the study herein is focused on the crystal structure of the KOR active-state for the discovery of novel KOR ligands using VS (Figure 1).

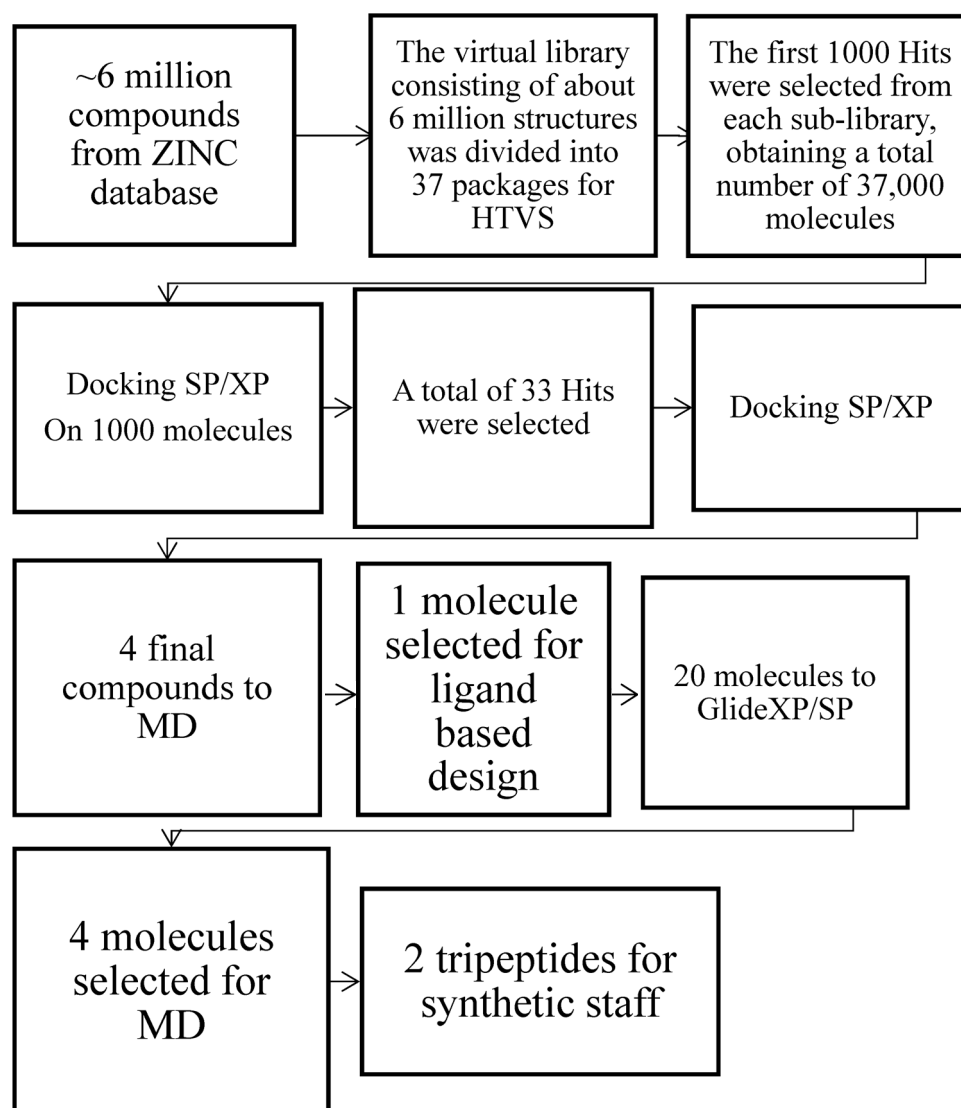


**Figure 1.** Computational workflow for the identification of the best two hits via Glide XP/SP and MD simulations.

Our computational protocol allowed us to identify two best hits as tripeptides that were synthesized in solution following standard peptide protocol synthesis [41,42]. The two compounds obtained in modest yields and excellent purity were also tested in vivo.

A comparison with other opioid receptor structures identifies residues critical for KOR activation and highlights the key molecular characteristics of subtype selectivity and signal bias.

The basic scaffolds JDtic and MP1104 take distinctive poses, although with common characteristics typical of opioid ligands: (1) anchoring in the receptor binding pocket through a saline bridge with D138 in TM3; (2) interaction with TM5 through a phenolic group; (3) forming interactions with TM2/3 through chemically different portions [43,44]. The JDtic antagonist and the MP1104 agonist both form a saline bridge between their respective amino and D138 receptor patterns as observed in many GPCR-ligand complexes. The greater distance of this saline bridge (3.0 Å) compared to similar interactions in KOR-JDtic (2.6 Å) and MOR-BU-72-Nb39 (2.7 Å) involves a weaker ionic interaction between MP1104 and KOR. D138 also forms a hydrogen bonding network with T1112.56 and Y3207.43 in KOR-MP1104-Nb, which is probably critical for full KOR activation; additionally, the mutation of these residues strongly attenuate or delete  $\beta$  arrestin2-recruitment mediated by MP1104 or Dynorphin A 1–17, respectively. The phenolic groups MP1104 and JDtic extend towards TM5, forming hydrogen bonds mediated by water with the backbone of the K227 carbonyl oxygen. This interaction was proposed to simulate the *N*-terminal tyrosine found in endogenous opioid peptides [45–47].

Directing the orientation of a rigid and hindered structure inside the binding pocket is fundamental to determine the effectiveness/strength of the ligand by minor changes in contact forces or tensions generated by substituents [48]. The orientation within the pocket probably depends (i) on the hybridization of the intramolecular bonds that determine the angles between the functional modules of the compound and (ii) specific interactions of the receptor subtype. Consequently, even small changes to identical scaffolds can subtly affect the compound binding pose, its potency, and/or effectiveness, as observed for other GPCR ligands [49].

## 2. Results and Discussion

### 2.1. Structure Based Design

The dipeptide H-D-Tyr-Val-NH<sub>2</sub> (ZINC71788314) obtained from virtual screening, presents interesting features: (a) a favorable docking score, with a value of  $-8.592$ ; (b) structural simplicity, which allows an easy *in silico* optimization process and a feasible synthetic process; (c) amino-terminal tyrosine residue, essential for an optimal interaction with the opioid receptor [50]. Thus it was considered as the lead compound for the further development of KOR ligands. In the first attempt, a lipophilic portion was inserted, represented by a benzyl group bonded to the carboxy-terminal, in order to stabilize the ligand at the orthosteric site of the receptor through the formation of hydrophobic interactions [51]. The different combinations of the D and L amino acids in the dipeptide tyrosyl-valine benzyl ester were considered for the calculations with Glide SP and XP docking methods. Then the elongation of the dipeptide's carboxy-terminal was taken in consideration, through the insertion of valine (Table 1) or tryptophan (Table 2) in the third position. The latter were considered by virtue of their chemical-physical properties, with the aim of creating a hydrophobic cluster [52]. The amino acid sequences of the two tripeptides, Tyr-Val-Val-OBz and Tyr-Val-Trp-OBz, were modified by D and L amino acids, and a docking score was calculated for each of them. The best result in terms of docking score values was obtained for the sequence D-Tyr-L-Val-L-Val-OBz, which was assumed as lead compound for further modification. The third approach consisted in the insertion of a bromine in *meta* position on the C-terminal aromatic ring. This modification was carried out with the aim of increasing the lipophilicity of the molecule intensifying the hydrophobic interactions between the C-terminal portion and the receptor pocket [53]. Both D and L series were considered in the docking prediction (Table 3).

**Table 1.** Docking score values for the designed peptides based on the insertion of valine in third position (second approach).

Peptides Sequences	Docking Score
D-Tyr-L-Val-L-Val-OBz	−11.789
D-Tyr-D-Val-L-Val-OBz	−11.467
L-Tyr-L-Val-D-Val-OBz	−11.189
D-Tyr-D-Val-D-Val-OBz	−11.154
D-Tyr-L-Val-D-Val-OBz	−9.975
L-Tyr-D-Val-D-Val-OBz	−9.598
L-Tyr-L-Val-L-Val-OBz	−8.510
L-Tyr-D-Val-L-Val-OBz	−8.188

**Table 2.** Docking score values for the designed peptides based on the insertion of tryptophan in third position (second approach).

Peptides Sequences	Docking Score
D-Tyr-L-Val-L-Trp-OBz	−11.582
L-Tyr-D-Val-L-Trp-OBz	−11.075
D-Tyr-D-Val-L-Trp-OBz	−8.174
L-Tyr-L-Val-L-Val-OBz	−7.523

**Table 3.** Docking score values for the designed peptides based on the third approach.

Peptides Sequences	Docking Score
D-Tyr-L-Val-L-Val-O-(3-Br)-OBz	−11.288
D-Tyr-D-Val-L-Val-(3-Br)-OBz	−10.728
D-Tyr-L-Val-D-Val-O-(3-Br)-OBz	−9.849
L-Tyr-L-Val-D-Val-O-(3-Br)-OBz	−9.451
D-Tyr-D-Val-D-Val-O-(3-Br)-OBz	−9.150
L-Tyr-L-Val-L-Val-O-(3-Br)-OBz	−9.087
L-Tyr-D-Val-D-Val-O-(3-Br)-OBz	−8.792
L-Tyr-D-Val-L-Val-O-(3-Br)-OBz	−7.774

The peptides with the best docking score values were selected for the next phase of molecular dynamics (MD), which allows one to simulate and analyze the physical movements of atoms and groups of atoms within a molecular system. The final poses of the best tripeptides obtained by the Glide/XP docking method are reported below (Figure 2).

## 2.2. Molecular Dynamics Simulation

The simulation was conducted on the four peptides selected in the design phase: H-D-Tyr-Val-Val-OBz, H-D-Tyr-Val-Trp-OBz, H-D-Tyr-D-Val-Val-OBz, and H-D-Tyr-Val-Val-O-(3-Br)-Bz, which were submitted to the Desmond Molecular Dynamic System [54] feature and incorporated into Maestro 2017. RMSD analysis provides information on the stability of the ligand within the active site of the receptor (Figures 3 and 4). The P-RMSF allows one to visualize the areas of the protein chain that fluctuate the most during the simulation, while the L-RMSF shows how the ligand fragments interact with the protein and determine its entropic role during the binding process. The bonds established between receptor and ligand have been evaluated and classified into four categories: (a) hydrogen bonds, (b) hydrophobic interactions, (c) ionic bonds, and (d) aqueous bridges, which mediate the interactions between the ligand and amino acid residues of the receptor. Below are the RMSD values of the four designed tripeptides and the crystallographic ligand (Figure 3).

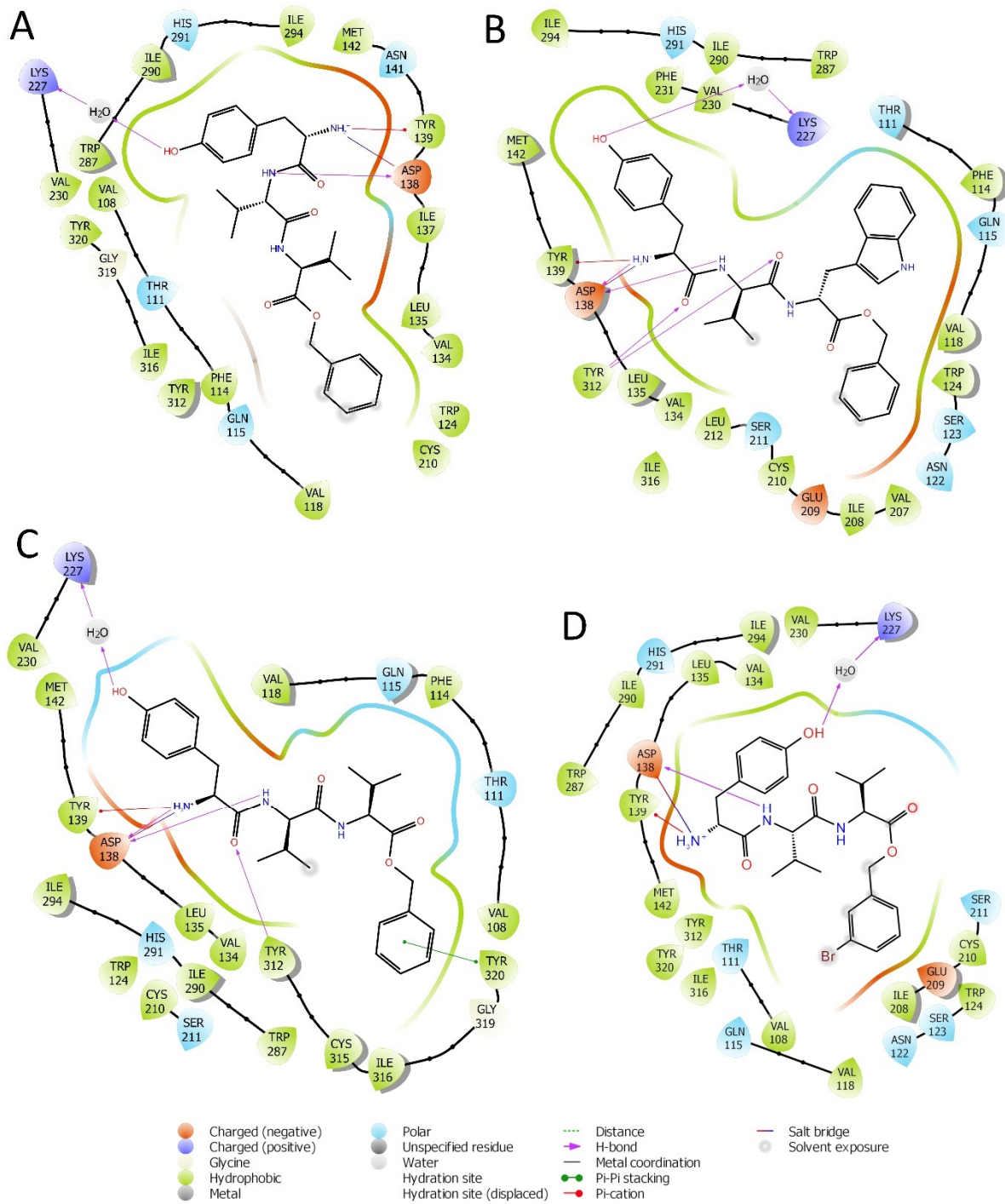


**Figure 2.** Interactions of peptides H-D-Tyr-Val-Val-OBz (A), H-D-Tyr-Val-Trp-OBz (B), H-D-Tyr-D-Val-Val-OBz (C), and H-D-Tyr-Val-Val-O-(3-Br)-Bz (D) with the amino acids residues of KOR binding site.

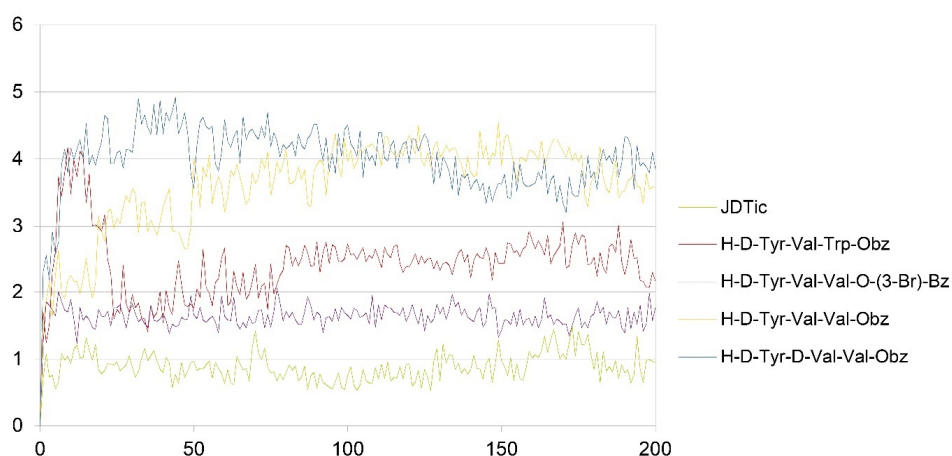


Figure 3. RMSD values of JDtic and the designed peptides (x axis: RMSD in Angstrom; y axis: time in ns).

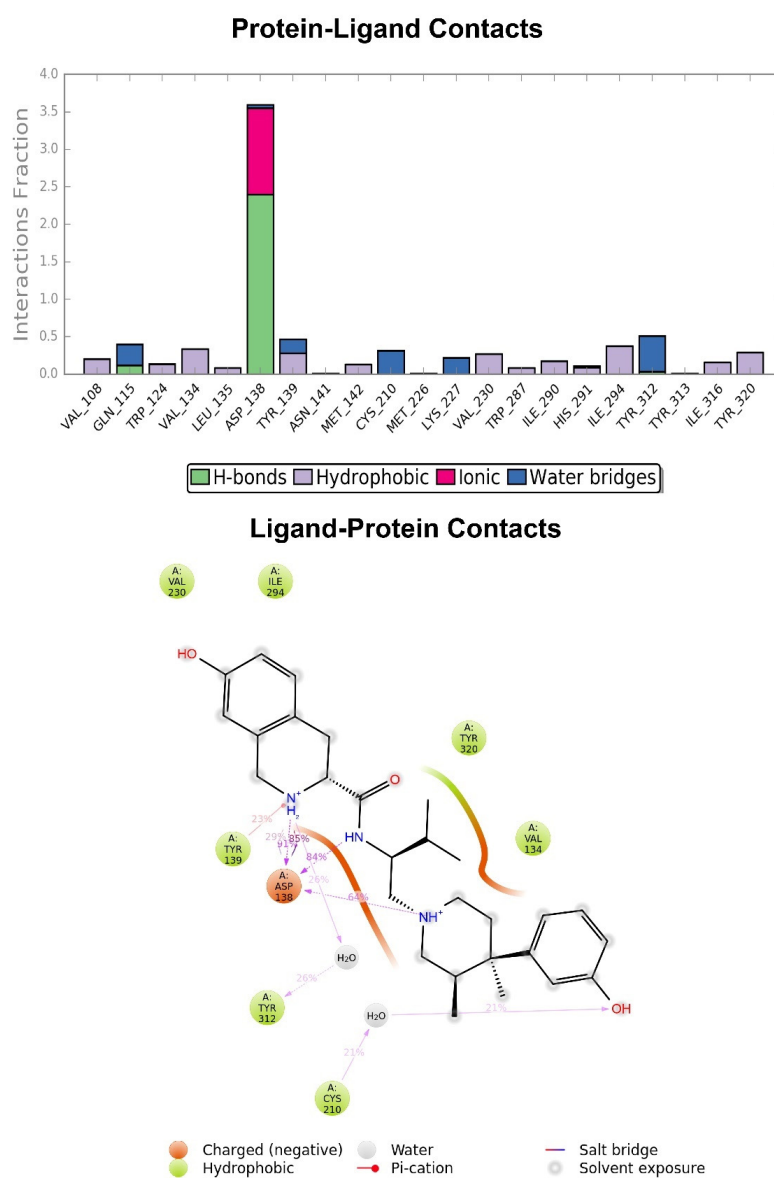


Figure 4. Graphic representation of the interactions between the JDtic and KOR binding site, expressed in %. Hydrogen bonds are in violet lines.

The crystallographic ligand has a stable pose inside the receptor pocket, as can be seen from the RMSD in Figure 3. The protein–ligand interactions are mainly represented by hydrogen bonds and the ionic nature with the residue of Asp138. The water bridge with the residue of Lys227, present both in the original pose and in the docked pose, was lost during the simulation (Figure 4). In the P-RMSF are reported the areas of the protein most affected by fluctuations, which exceeded the value of 4.5 Å (Figure 5). JDtic does not show fluctuations greater than 1.0 Å, except for one of the two methyl groups linked to the isopropyl fragment (fragment 16), which reaches values greater than 1.5 Å (Figure 5).

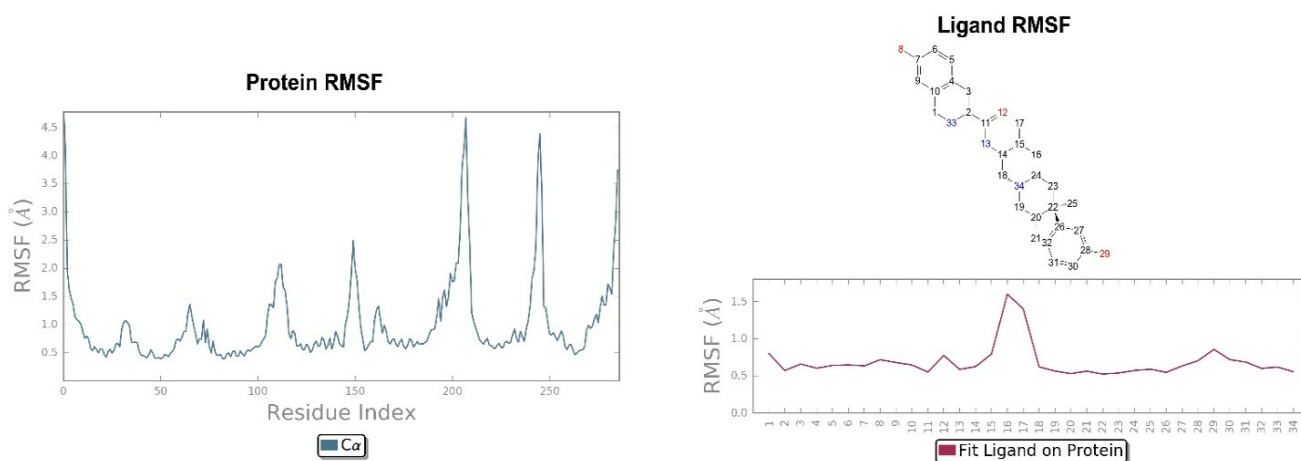


Figure 5. On the left: P-RMSF for KOR; on the right: L-RMSF of JDtic.

The RMSD of the H-D-Tyr-Val-Val-OBz tripeptide located in the receptor active site appears to stabilize after 4 ns (Figure 3). The interactions with the KOR are better than in JDtic. In addition to the numerous hydrogen bonds and ionic interactions involving the Asp138 residue, there are further stabilizations of the ligand through different hydrophobic interactions with Tyr139 and Trp287 (Figure 6). Interestingly the water bridge is established between the phenolic hydroxyl group of D-Tyr and the Hys291 residue of the protein. The P-RMSF illustrates the fluctuations of the protein at slightly higher values (5.6 Å) than that found in JDtic (Figure 7). In the L-RMSF graph the best fluctuations are recorded for the side chain of the valine at the C-terminal end (fragment 24) (Figure 7).

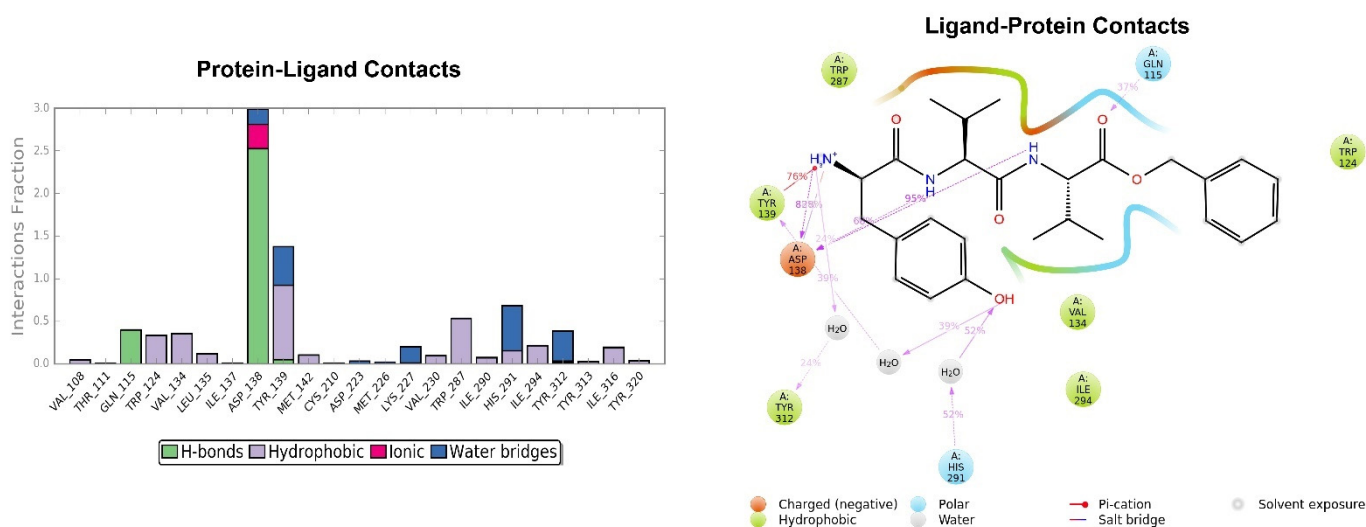


Figure 6. Representation of the main interactions found for H-D-Tyr-Val-Val-OBz in the KOR binding site, expressed in %. Hydrogen bonds are in violet lines.

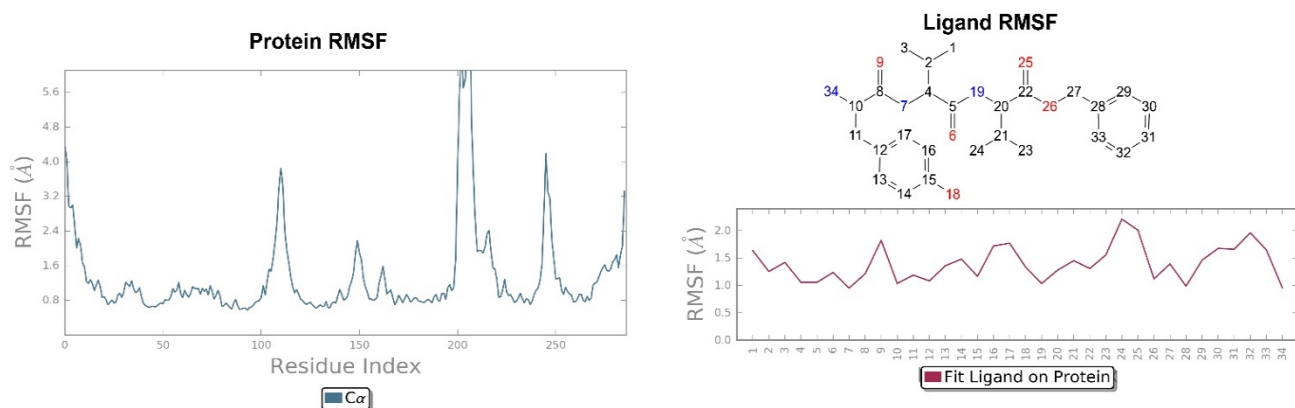


Figure 7. On the left: P-RMSF, receptor kappa; on the right: L-RMSF di H-D-Tyr-Val-Val-OBz.

Looking at Figure 8, the tripeptide H-D-Tyr-Val-Val-O-(3-Br)-Bz (6) turns out to be the ligand with the most stable profile during the simulation time. The receptor–ligand interactions are mainly characterized by hydrogen bonds with Asp138 and Gln115, with multiple hydrophobic interactions involving non-polar amino acid residues, such as Ile294 and Val118. Similarly to the tripeptide analyzed previously, there is interaction with the Hys291 residue assisted by a water molecule (Figure 8). The P-RMSF graph is comparable to the previous one (Figure 9); while the highest fluctuations are in correspondence with the aromatic ring replaced with the bromine atom (fragments 28–33 and 34).

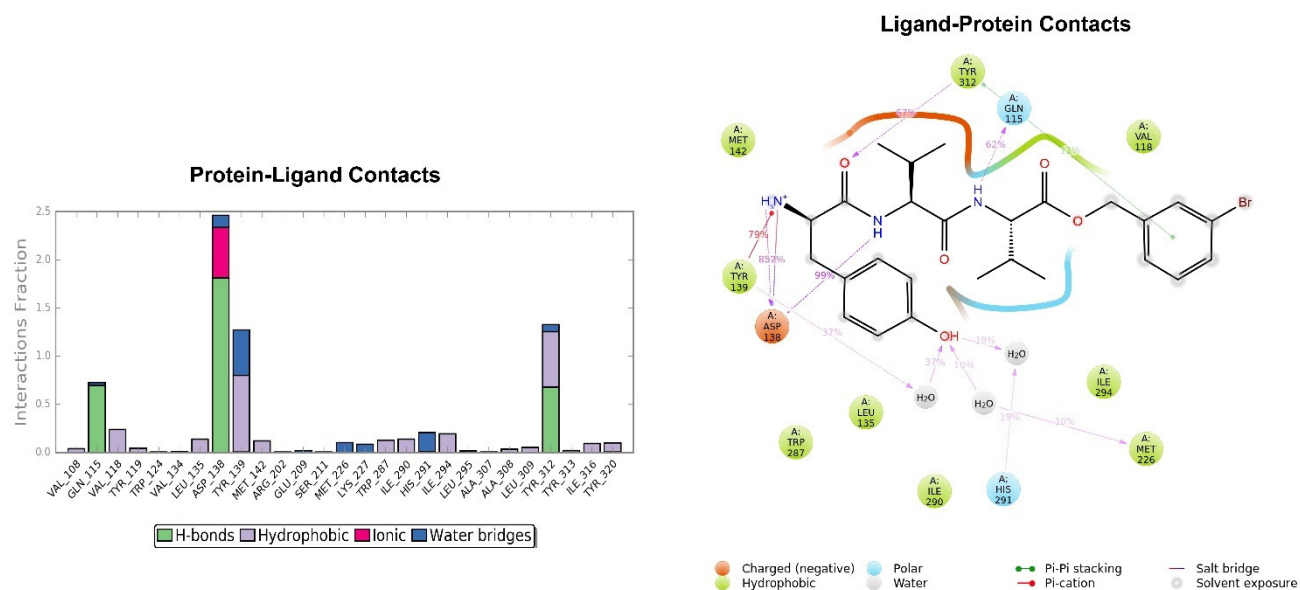
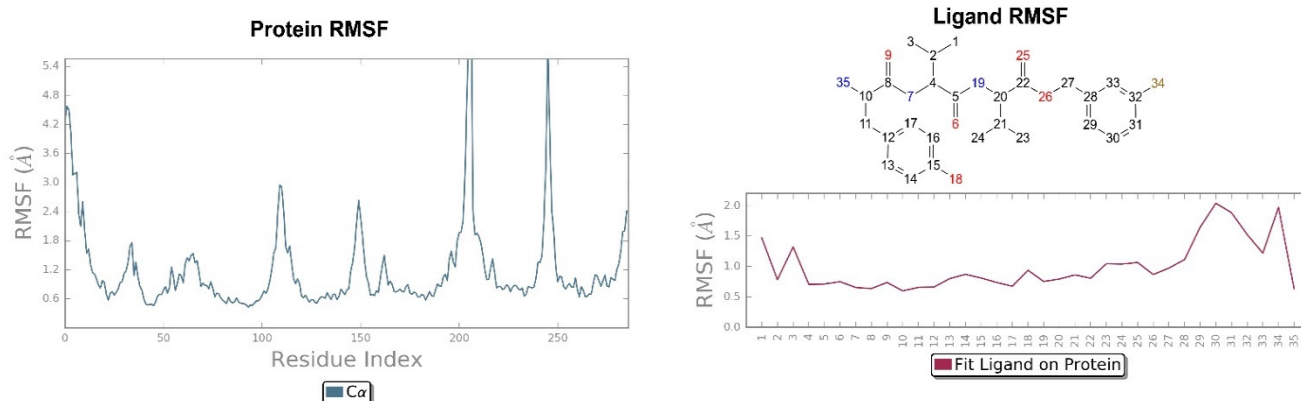
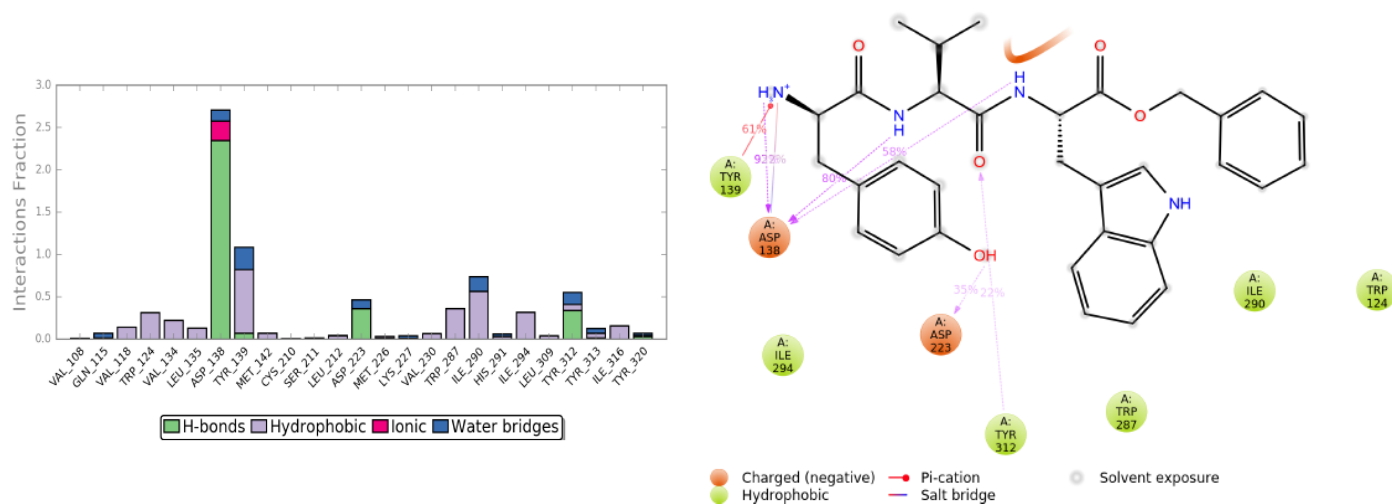


Figure 8. Key interactions of H-D-Tyr-Val-Val-O-(3-Br)-Bz (6) with KOR binding pocket expressed in %. Hydrogen bonds are in violet lines.



**Figure 9.** On the left: P-RMSF, KOR; on the right: L-RMSF of H-D-Tyr-Val-Val-O-(3-Br)-Bz (6).

The pose of H-D-Tyr-Val-Trp-OBz (**11**) is generally stable during molecular dynamics, and the binding with the KOR mainly focuses on hydrogen interactions with Asp138. The additional interactions of a hydrophobic nature allow for a good stabilization of the molecule within the receptor site; however, the hydrogen bond with the catalytic water molecule that acts as a bridge with the Lys227 residue is lost (Figure 10). The P-RMSF graph is comparable to the previous ones, and, in the L-RMSF, the main fluctuations are observed for fragments 25–31, due to the C-terminal benzyl group (Figure 11).



**Figure 10.** Interactions of H-D-Tyr-Val-Trp-OBz (**11**) within the KOR binding pocket, expressed in %. Hydrogen bonds are in violet lines.

The pose of the tripeptide H-D-Tyr-D-Val-Val-OBz is stable and characterized by the prevalence of a hydrogen bond between the NH group of the backbone and the Asp138 residue. Interestingly the *N*-terminal group of tyrosine is involved in the hydrogen bond with Asp138 and a water molecule (Figure 12); the benzyl ring established a  $\pi$ - $\pi$  stack interaction with Tyr320 and hydrophobic contacts with Val108, Trp287. The key interaction between the hydroxyl group of Tyr and His291 is also present. The highest fluctuations occur at the valine-O-benzyl portion (fragments 25–34) of the peptide (Figure 13).

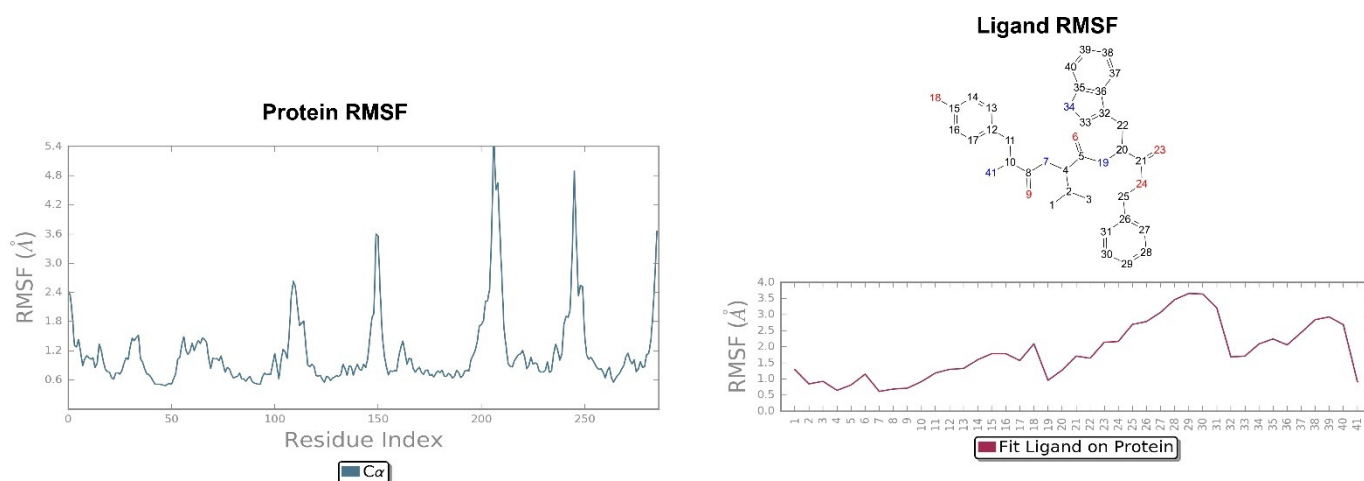


**Figure 11.** On the left: P-RMSF of KOR; on the right: L-RMSF of H-D-Tyr-Val-Trp-OBz (11).

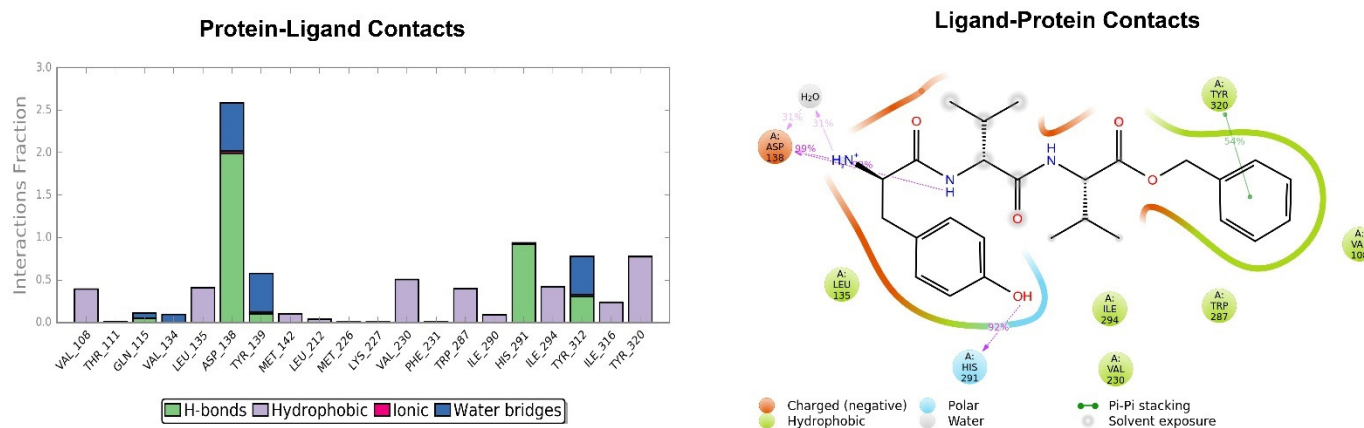


**Figure 12.** Interactions of H-D-Tyr-D-Val-Val-OBz within the KOR binding pocket, expressed in %. Hydrogen bonds are in violet lines.

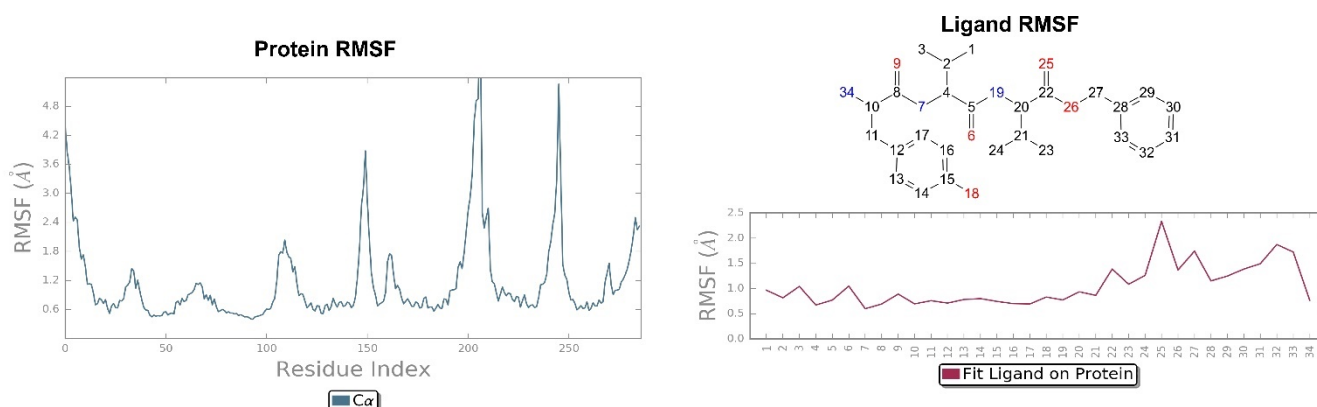


**Figure 13.** On the left: P-RMSF for KOR; on the right: L-RMSF of H-D-Tyr-D-Val-Val-OBz.

To conclude tripeptides H-D-Tyr-Val-Val-O-(3-Br)-Bz (6) and H-D-Tyr-Val-Trp-OBz (11) are of great interest because they exhibit enhanced docking score values compared to the original dipeptide H-D-Tyr-Val-NH<sub>2</sub> (−11.288 and −11.582 respectively, Tables 2 and 3), higher than that of the crystallographic ligand (−11.176 with Glide/XP). The tripeptides designed *in silico* show strong stability, preserve the key interaction with the Asp138 residue,

and are stabilized by efficient additional hydrophobic interactions. Thus, they were selected for solution phase peptide synthesis and further tested *in vivo* by means of tail flick and formalin tests.

### 2.3. Antinociceptive Effect *In Vivo*

The results obtained in the tail flick and in the formalin tests are reported in Figure 14. In the tail flick test, the administration of tripeptides **6** and **11** induced antinociceptive effects that peaked 30 min after the administration (Figure 14, left panel). After the peak time, compound **6** induced significant antinociceptive effect at 45 min after the administration, then its effect declined to MPE values similar to those observed in vehicle-treated animals 90–120 min thereafter. On the contrary, peptide **11** induced antinociceptive effects that were still significant at 45, 60, and 90 min after administration. The results obtained in the formalin test are reported in Figure 14, right panel. In the early phase of the formalin test, both **6** and **11** were able to reduce the nociceptive behavior induced by aldehyde. When the late phase was recorded, only compound **11** was able to reduce the licking nociceptive behavior induced by formalin, whereas compound **6** was ineffective. All together these data highlight a better antinociceptive effect for peptide **11** compared to **6** in both tests. The inflammation process contributes to the second phase of the test, during which compound **11** is still active, indicating an acute response to a model of ongoing acute pain involving inflammation and aspects of central sensitization. This could be due either to a good penetration of the blood–brain barrier, as well as to the ability of this tripeptide to interact with opioid receptors at the periphery. With the aim of shedding some light on the possible pharmacokinetic profiles of these two compounds, an ADME study was performed *in silico* by means of SwissADME free web tool (<http://www.swissadme.ch/index.php>, accessed on 8 February 2021) [52].

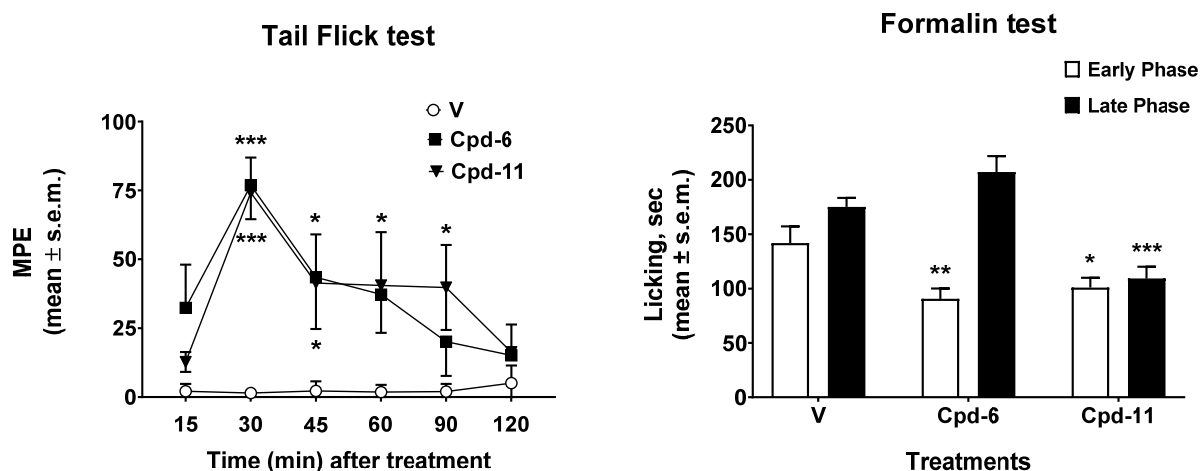


**Figure 14.** Effects induced by compounds **6** and **11** in the tail flick (left panel) and in the formalin (right test) tests. In the tail flick test, compounds were injected *i.c.v.* at a dose of 0.6 nmol/10  $\mu$ L. In the formalin test, compounds were injected *s.c.* in the dorsal surface of the hind paw, 15 min before formalin. V is for vehicle-treated animals. \* is for  $p < 0.05$ ; \*\* is for  $p < 0.01$ ; \*\*\* is for  $p < 0.001$ .  $N = 7$ .

### 2.4. *In Silico* ADME and Drug-Likeness Evaluation

The best two tripeptides **6** and **11** were submitted to an *in silico* evaluation of ADME (adsorption, distribution, metabolism, excretion) properties to estimate their pharmacokinetics and drug-likeness (Table 4).

**Table 4.** *in silico* ADME study for peptides 6 and 11.

Peptides	Lipophilicity		Drug-Likeness		Pharmacokinetics		
	TPSA (Å)	CLogP (o/w)	Bioavailability Score	Lipinski Filter	GIA	P-gp Substrate	CYP3A4 Inhibitor
6	132.37	2.59	0.55	Yes (1)	high	yes	no
11	148.16	2.46	0.55	Yes (1)	low	yes	yes

Abbreviations: CLogP (o/w), logarithm of compound partition coefficient between n-octanol and water; CYP3A4, cytochrome P450 3A4; GIA, gastrointestinal absorption; Lipinski filter (with number of violations in bracket); TPSA, topological polar surface area.

Prediction of GIA is based on the brain or intestinal estimated permeation (BOILED-egg) model, which calculates the passive gastrointestinal absorption and blood–brain barrier penetration (Figures S5 and S6 in Supplementary Materials). This was high for peptide 6 and low for 11; however, both of them show the same bioavailability score (0.55); this could be due to the fact that they turn out to be good substrates for P-glycoprotein, which is a cell membrane transport protein responsible for pumping drugs out [54–56]. Moreover, peptide 11 showed inhibition of CYP3A4, an enzyme involved in the metabolism of drugs [54], while peptide 6 lacks this interaction, which could prevent the accumulation of drugs. Peptides 6 and 11 have more than 10 rotatable bonds and a TPSA value > 130 Å (Table 4), indicating a low oral bioavailability [56]; in fact, both values of POLAR (TPSA) and FLEX for 6 and 11 are outside the desired range for improved bioavailability (Figures S5 and S6). Overall, this *in silico* study indicates slightly better pharmacokinetic properties for 6 compared to 11 but similar lipophilicity, which reflects their poor predicted bioavailability.

### 3. Methods and Materials

#### 3.1. Library Preparation

The virtual library of compounds was retrieved from the ZINC database [57], from which a subset of ~6 million commercially available molecules were selected using the following filtering criteria: (i) molecules with molecular weight between 150 and 500; (ii) log P less than or equal to 5; (iii) hydrogen binding donor groups less than or equal to 5; (iv) hydrogen binding acceptor groups lower than or equal to 10; (v) PSA (molecular polar surface area) less than 150 and rotatable bonds less than or equal to 7. Compounds containing extremely reactive functional groups were discarded, e.g., thiol groups, Michael acceptors, and aldehyde groups.

The selected molecules in MOL2 format were submitted to LigPrep tool [58], incorporated in Maestro Schrödinger 2017-1 [59]. LigPrep allows one to generate accurate and energetically minimized 3D structures, following these parameters: (i) the addition of any absent hydrogen atoms; (ii) the removal of unwanted molecules (water, salts); (iii) the neutralization of all groups, before generating the states of ionization with the Epik [60] function, setting a pH range of 7.4 +/- 0.0, with the aim of replicating physiological conditions. The final steps of this process consist in the generation of a series of tautomers for each structure, preserving the stereochemistry of the chiral centers of the ligands.

#### 3.2. Protein Preparation

The human KOR (PDB code 4DJH) was retrieved from PDB in complex with a selective antagonist JD1c ((3R)-7-hydroxy-N-[(2S)-1-[(3R,4R)-4-(3-hydroxyphenyl)-3,4-dimethylpiperidin-1-yl]-3-methylbutan-2-yl]-1,2,3,4-tetrahydroisoquinoline-3-carboxamide) [6]. The Protein Preparation Wizard tool embedded in Maestro 2017-1 [61] allows for the accurate conversion of the raw PDB file into a fully prepared protein structure. During this phase, hydrogen atoms were added to all protein residues, and three of the four chains were removed from the crystallized structure, retaining only the A chain containing the binding cavity. Then, hydrogen bonds and residue protonation states were refined by setting the pH to 7.4 with the PropKa function [62]. The minimization was carried out using the force field OPLS3 [63].



(v) biological activity: the possible presence of biologically active molecular structures has been investigated in the literature. A total of 33 hits were selected, of which 10 with the best docking score values, 10 with interesting additional interactions, 10 with the best degree of overlap with JDTic and 3 with biological activity previously reported in literature [65–67]. Further docking optimization was done using Glide, which allows the ligand to be anchored to the active site of the receptor, providing for its binding mode. The previously created grid was selected, and two scoring functions with increasing precision were adopted: SP and XP Glidescore. We opted for a flexible docking model, leaving unchanged the standard Scaling factor parameters equal to 0.80 on the Van der Waals radii of the non-polar atoms of the receptor, defined as the atoms whose absolute value of the partial atomic charge ( $\delta - \text{o } \delta +$ ) is positive and with a maximum value of 0.15. The ZINC04632302 outcome is a benzimidazole that was characterized in vitro on MOR and DOR [68] and the compound ZINC06697859, which expressed antagonist activity with a high affinity for KOR ( $K_i = 0.09 \mu\text{M}$ ) [69]. The ZINC71788314 is a D-tyrosyl-valinamide (H-D-Tyr-Val-NH<sub>2</sub>), a dipeptide obtained from the  $\alpha$ -amidation process of the synthetic peptide D-tyrosyl-valyl-glycine (H-D-Tyr-Val-Gly-OH) in the brain [70].

### 3.6. Molecular Dynamics

The simulation was conducted on the four peptides H-D-Tyr-Val-Val-OBz, H-D-Tyr-Val-Trp-OBz, H-D-Tyr-D-Val-Val-OBz, and H-D-Tyr-Val-Val-O-(3-Br)-Bz through the Desmond Molecular Dynamic System [60–71] feature incorporated into Maestro 2017-1.

The system builder instrument in Desmond was used for the preparation of receptor–ligand complexes; the lipid bilayer membrane DPPC was set at 325 K, through which the various complexes to be examined were inserted. The entire system was centered by an orthorhombic box of 302,956 Å<sup>3</sup> after minimization, which was saturated with water molecules by setting the TIP3P aqueous solvent model, in order to recreate physiological conditions. In the “Ions” section, the NaCl salt at a concentration of 0.15 M was added and the OPLS3 force field set.

The resulting system, displayed in the Workspace, was loaded in the “Molecular Dynamics” panel, belonging to the Desmond package. For each protein–ligand system, the overall simulation time was 20 ns, with an approximate number of frames equal to 200. For the ensemble option, which represents the macroscopic conditions of the system, the statistical set NPT (ensemble isothermal-isobaric), characterized by constant values of the number of particles, pressure, and temperature. In each molecular dynamics, the following parameters have been set: (a) temperature at 309.15 K and (b) pressure at 1.01325 bar. Newton’s equations of motion in the molecular dynamics trajectory were integrated with the r-RESPA method. Constraints have been placed on atoms capable of participating in hydrogen interactions, as they determine higher frequency vibrations, causing a restriction of the integration step (time-step) to about 0.5fs in an MD. Therefore the SHAKE method was used, reaching an integration step of 2 fs [70]. The contribution of the short range electrostatic interactions and the Lennard-Jones potential was evaluated by applying a spherical cut-off of 10 Å. Instead, the contribution of long-range electrostatic interactions, represented by the summation of the pairs of unbound atoms of the system, was estimated using the particle mesh Ewald method [71,72].

### 3.7. Chemistry

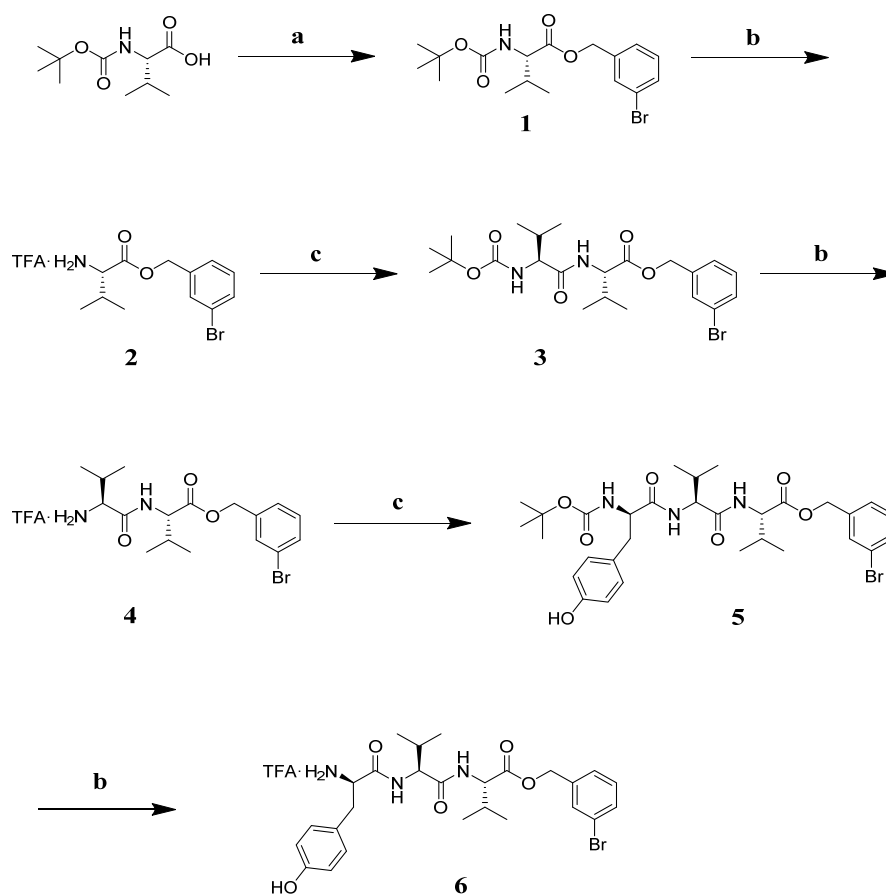
#### 3.7.1. General

All the reagents and amino acids for the synthesis were purchased from Sigma Aldrich (Milan, Italy). Final products were purified in RP-HPLC using a Waters XBridge™ Prep BEH130 C18 column, 5.0  $\mu\text{m}$ , 250 mm  $\times$  10 mm at a flow of 4 mL/min, and a Waters 600 binary pump (Milford, MA, USA), using as eluent a linear gradient of H<sub>2</sub>O/ACN 0.1% TFA, starting from 5% ACN to 90% ACN in 35 min. The nature of the protected N <sup>$\alpha$</sup> -Boc(D)Tyr-Val-Val-O-(3-Br)-Bz and N <sup>$\alpha$</sup> -Boc(D)Tyr-Val-Trp-OBz was confirmed by NMR with a Varian Inova 300 MHz instrument and ESI-LRMS Thermo Finnigan mass spectrom-

etry (Somerset, NJ, USA). The purity of all final products as TFA salts was confirmed by NMR analysis, ESI-LRMS, and analytical RP-HPLC (C18-bonded 4.6 × 150 mm; 1 mL/min; 0.1% H<sub>2</sub>O/ACN gradient TFA from 5% to 95% ACN in 30 min), and the results were ≥95%.

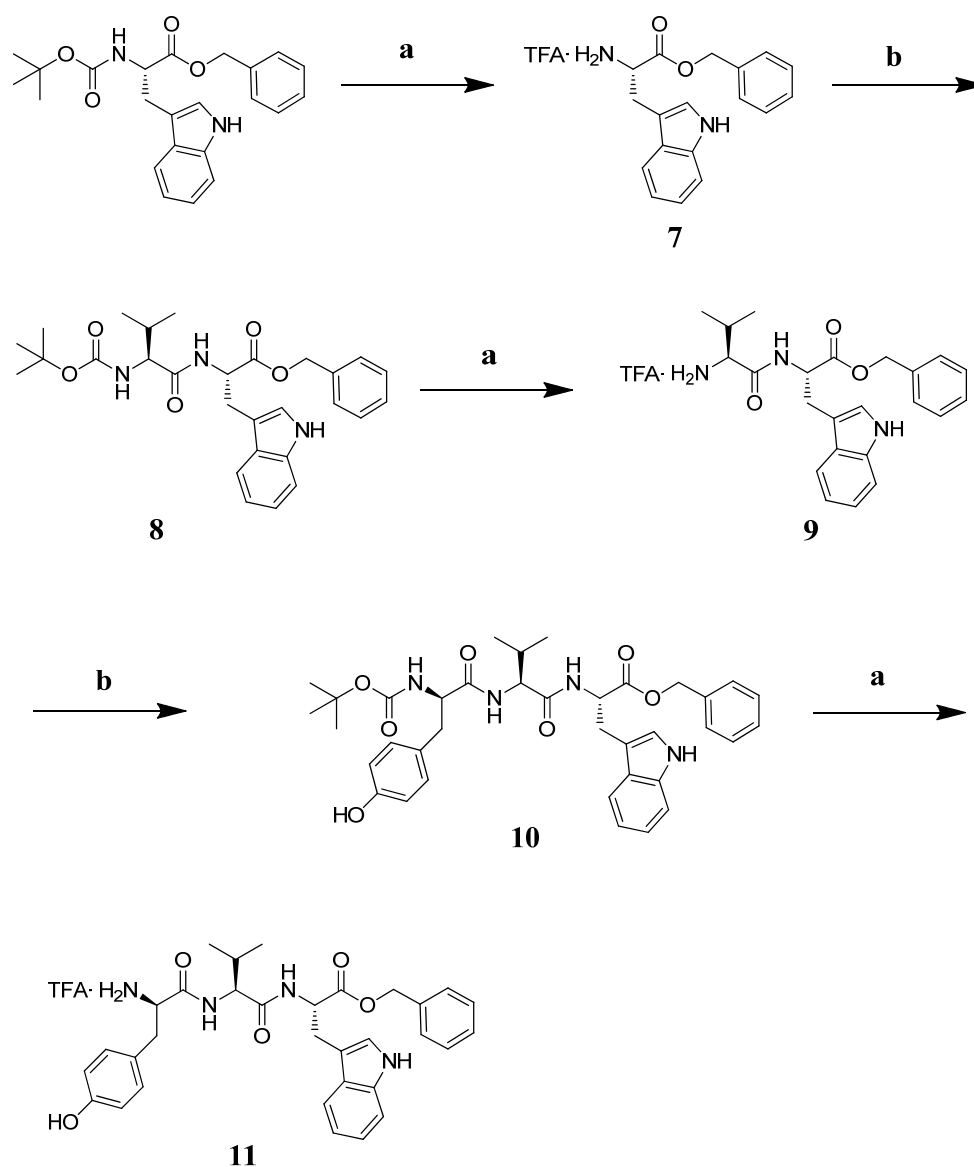
### 3.7.2. Synthesis

The tripeptide TFA·NH<sub>2</sub>-(D)Tyr-Val-Val-O-(3-Br)-Bz (**6**) was obtained starting from Boc-Val-OH, which was involved in a benzylation reaction with 3-bromo-benzyl, K<sub>2</sub>CO<sub>3</sub> at reflux in ACN for 4 h. Intermediate **1** was deprotected with a mixture TFA:DCM = 1:1 at r.t. under stirring for 1 h. Intermediate **2** was reacted with Boc-Val-OH, EDC·HCl, HOBT and DIPEA in DMF at r.t. for 2 h. Repeated deprotection and coupling steps afforded Boc-protected intermediate **5** [73]. This peptide was treated with the TFA/DCM mixture so as to obtain the desired final product **6** as a TFA salt (Scheme 1).



**Scheme 1.** Reagents and conditions: (a) K<sub>2</sub>CO<sub>3</sub> (1.2 eq), 3-bromo-benzyl (1 eq), ACN (5 mL), reflux, 4 h; (b) TFA:DCM = 1:1, r.t., 1 h; (c) EDC·HCl (1.1 eq), HOBT (1.1 eq), Boc-Val-OH for **2** or Boc-Tyr-OH for **5** (1 eq), DIPEA (3 eq), in DMF r.t. 12 h.

The tripeptide TFA·NH<sub>2</sub>-D-Tyr-Val-Trp-OBz (**11**) was prepared in solution starting from Boc-Trp-OBz. The amino acid was deprotected with a mixture of TFA: DCM = 1: 1 at r.t. for 1 h and subsequently reacted with Boc-Val-OH in DMF, EDC·HCl, HOBT, and DIPEA at r.t. for 12 h. Intermediate **8** was deprotected and reacted with Boc-D-Tyr-OH under the aforementioned conditions. The final product **11** was obtained following the removal of the *tert*-butyloxycarbonyl group with an overall yield of 5.86% (Scheme 2).



**Scheme 2.** Reagents and conditions: (a) TFA:DCM = 1:1, r.t. 1 h; (b) EDC·HCl (1.1 eq), HOBT (1.1 eq), Boc-Val-OH or 9, or Boc-D-Tyr-OH (1 eq) for 10, DIPEA (3 eq), in DMF, r.t. 12 h.

### 3.7.3. Characterization of Peptides and Intermediates

**Boc-Val-O-(3-Br)-Bz (1).** Boc-Val-OH (100 mg, 0.46 mmol) was dissolved in ACN (5 mL) with K<sub>2</sub>CO<sub>3</sub> (69.65 mg, 1.2 eq) and 3-bromo-benzyl (104.97 mg, 1 eq). The mixture was left to reflux for 4 h., checking the completeness of the reaction with TLC (100% DCM). The solvent was removed in vacuum giving a raw material pure in TLC (100% DCM, R<sub>f</sub> = 0.3) in 92% yield. <sup>1</sup>H NMR (CDCl<sub>3</sub>) δ: 7.45 (m, 2H, aromatics); 7.25–7.20 (m, 2H, aromatics); 5.17–4.98 (m, 3H, NH<sup>α</sup> + CH<sub>2</sub> benzyl), 4.27 (m, 1H, CH<sup>α</sup>), 2.13 (m, 1H, CH<sup>β</sup>), 1.43 (s, 9H, Boc), 0.94 (d, 3H, CH<sub>3</sub>), 0.84 (d, 3H, CH<sub>3</sub>).

**TFA·NH<sub>2</sub>Val-O-(3-Br)-Bz (2).** Intermediate 1 was treated with a mixture of TFA:DCM = 1:1 stirring for 1 h at r.t. then the solvent was removed in a rotary evaporator, washed with DCM (5 times), dried in high vacuum, and used as such in the next step without further purification.

**Boc-Val-Val-O-(3-Br)-Bz (3).** Boc-Val-OH (90.81 mg, 1.1 eq) was dissolved in DMF (15 mL) at 0 °C, stirring for 5 min, then EDC·HCl (80.51 mg, 1.1 eq) and HOBT (56.75 mg, 1.1 eq) were added. After 10 min, intermediate 2 (149.10 mg, 0.38 mmol) and DIPEA (0.2 mL, 3 eq)

were added, stirring at 0 °C for 10 min., then at r.t. for 12 hs. After a standard work-up, the desired peptide was obtained in 68% yield, pure in TLC (DCM:AcOEt = 1:1;  $R_f$  = 0.2).

TFA·NH<sub>2</sub>-Val-Val-O-(3-Br)-Bz (4). Intermediate 3 was deprotected following the same procedure reported for intermediate 2, and used as is without further purification.

Boc-D-Tyr-Val-Val-O-(3-Br)-Bz (5). Dipeptide 4 as a TFA salt was coupled with Boc-D-Tyr-OH (84.39 mg, 1.1 eq), following the procedure previously reported for peptide 3. The Boc-protected peptide was purified on silica gel column (mobile phase AcOEt:DCM = 1:1). The desired product was obtained with 39.7% yield. LRMS for C<sub>31</sub>H<sub>42</sub>BrN<sub>3</sub>O<sub>7</sub>: calcd  $m/z$ : 647.2; found: 670.1 [M + Na]<sup>+</sup>.

TFA·NH<sub>2</sub>-D-Tyr-Val-Val-O-(3-Br)-Bz (6): Peptide 5 was treated with a TFA/DCM mixture following the procedure previously described, so as to give final peptide 6 as a TFA salt, the identity of which was confirmed through <sup>1</sup>H-NMR. <sup>1</sup>H-NMR (CDCl<sub>3</sub>) δ: 7.45 (m, 2H, aromatics); 7.25–7.20 (m, 9H, aromatics + NH<sub>3</sub><sup>+</sup>); 6.86 (d, 2H, aromatics); 6.61 (dd, 2H, 2\*NH<sup>α</sup>); 5.17–4.98 (m, 3H, NH<sup>α</sup> + CH<sub>2</sub> benzyl), 4.57 (m, 1H, CH<sup>α</sup> Val); 4.35 (m, 1H, CH<sup>α</sup> Tyr); 4.27 (m, 1H, CH<sup>α</sup> Val), 2.93 (m, 2H, CH<sub>2</sub><sup>β</sup> Tyr); 2.13 (m, 1H, CH<sup>β</sup> Val), 2.02 (m, 1H, CH<sup>β</sup> Val); 0.94 (d, 6H, CH<sub>3</sub>), 0.84 (d, 6H, CH<sub>3</sub>).

TFA·NH<sub>2</sub>-Trp-OBz (7). Boc-Trp-OBz was treated with a mixture of TFA:DCM = 1:1 at r.t. for 1 h and used as such for the next reaction.

Boc-Val-Trp-OBz (8). Boc-Val-OH (40.6 mg, 1.1 eq) was dissolved in DMF (7 mL) in an ice bath, stirring for 5 min. EDC·HCl (36.42 mg, 1.1 eq) and HOBt (25.68 mg, 1.1eq) were added; after 10 min, intermediate 7 (1.1 mg, 1 eq) and DIPEA (3 eq) were transferred into the reaction round bottom flask left at 0 °C for 10 min and at r.t. overnight. The desired product was obtained after a standard reaction work-up in 85% yield, pure in TLC (AcOEt:DCM = 1:9,  $R_f$  = 0.3).

TFA·NH<sub>2</sub>-Val-Trp-OBz (9). The Boc-protecting group was removed from 8 following the same procedure adopted for 7.

Boc-D-Tyr-Val-Trp-OBz (10). The coupling reaction among intermediate 9 (66 mg, 0.13 mmol) and Boc-Tyr-OH (39.38 mg, 1.1 eq) was setup following the procedure previously described. The so obtained crude peptide was purified on silica gel column (mobile phase 1:1 AcOEt:DCM) affording the pure peptide in 19.93% yield (AcOEt:DCM = 1:1;  $R_f$  = 0.3). The identity was confirmed by LRMS and <sup>1</sup>H-NMR. LRMS for C<sub>37</sub>H<sub>44</sub>N<sub>4</sub>O<sub>7</sub>: calcd  $m/z$ : 656.3; found  $m/z$ : 679.2 [M + Na]<sup>+</sup>. <sup>1</sup>H-NMR (CDCl<sub>3</sub>) δ: 8.27 (s, 1H, NH indolic); 7.51 (d, 1H, Trp indolic); 7.32–7.07 (m, 6H, aromatics Trp + NH<sup>α</sup> Trp + NH<sup>α</sup> Val); 6.68 (d, 2H, Tyr aromatics); 6.48 (d, 2H, Tyr aromatics); 6.32 (d, 1H, Boc NH); 4.92 (s, 1H, CH<sub>2</sub> benzyl); 4.94–4.90 (m, 1H, CH<sup>α</sup> Tyr); 4.19–4.17 (m, 2H, CH<sup>α</sup> Trp, Val); 2.95–2.88 (m, 4H, CH<sup>β</sup> Tyr, Trp); 1.96 (m, 1H, CH<sup>β</sup> Val); 1.39 (s, 9H, 3\*CH<sub>3</sub>); 0.79–0.65 (dd, 6H, 2\*CH<sub>3</sub> Val).

TFA·NH<sub>2</sub>-D-Tyr-Val-Trp-OBz (11). Boc-D-Tyr-Val-Trp-OBz 10 was treated with a mixture of TFA/DCM = 1:1 at r.t. for 1 h. The so-obtained product as a TFA salt was purified on RP-HPLC, and the structure was confirmed with <sup>1</sup>H-NMR. <sup>1</sup>H-NMR (CDCl<sub>3</sub>) δ: 10.96 (s, 1H, OH Tyr); 8.27 (s, 1H, NH indolic); 7.99 (s, 3H, NH<sub>3</sub><sup>+</sup> Tyr); 7.51 (d, 1H, Trp indolic); 7.32–7.07 (m, 6H, aromatics Trp + NH<sup>α</sup> Trp + NH<sup>α</sup> Val); 6.68 (d, 2H, Tyr aromatics); 6.48 (d, 2H, Tyr aromatics); 4.92 (q, 1H, CH<sub>2</sub> benzyl); 4.94–4.90 (m, 1H, CH<sup>α</sup> Tyr); 4.19–4.17 (m, 2H, CH<sup>α</sup> Trp, Val); 2.95–.88(m,4H, H<sup>β</sup> Tyr, Trp); 1.96 (m, 1H, CH<sup>β</sup> Val); 0.79–0.65 (dd, 6H, 2\*CH<sub>3</sub> Val).

### 3.8. In Vivo Assays

#### 3.8.1. Animals

In our experiments, we used CD-1 male mice (Charles River, Italy, Sant'Angelo Lodigiano, 25–30 g) maintained in colony, housed in cages (7 mice per cage) under standard light/dark cycle (from 7:00 a.m. to 7:00 p.m.), temperature (21 ± 1 °C) and relative humidity (60% ± 10%) for at least 1 week. Food and water were available *ad libitum*. The

Service for Biotechnology and Animal Welfare of the Istituto Superiore di Sanità and the Italian Ministry of Health authorized the experimental protocol according to Legislative Decree 26/14.

### 3.8.2. Treatment Procedure

DMSO was purchased from Merck (Rome, Italy). Peptide solutions were freshly prepared using saline containing 0.9% NaCl and DMSO in the ratio DMSO/saline 1:5 *v/v* every experimental day. These solutions were injected at a volume of 10  $\mu\text{L}$ /mouse for intracerebroventricular (i.c.v.) administrations or at a volume of 20  $\mu\text{L}$ /mouse for subcutaneous (s.c.) administrations.

### 3.8.3. Surgery for Intracerebroventricular Injection

For i.c.v. injections, mice were lightly anesthetized with isoflurane, and an incision was made in the scalp, and the bregma was located. Injections were performed using a 10  $\mu\text{L}$  Hamilton microsyringe equipped with a 26-gauge needle, 2 mm caudal and 2 mm lateral from the bregma at a depth of 3 mm.

### 3.8.4. Tail Flick Test

The tail flick latency was obtained using a commercial unit (Ugo Basile, Gemonio, Italy), consisting of an infrared radiant light source (100 W, 15 V bulb) focused onto a photocell utilizing an aluminum parabolic mirror. During the trials, the mice were gently hand-restrained using leather gloves. Radiant heat was focused 3–4 cm from the tip of the tail, and the latency (s) of the tail withdrawal to the thermal stimulus was recorded. The measurement was interrupted if the latency exceeded the cut off time (15 s). The baseline latency was calculated as mean of three readings recorded before testing at intervals of 15 min and the time course of latency determined at 15, 30, 45, 60, 90, and 120 min after treatment. Data were expressed as the area under the curve of the maximum percentage effect (%MPE) = (post-drug latency – baseline latency)/(cut-off time – baseline latency)  $\times$  100.

### 3.8.5. Formalin Test

In the formalin test, the injection of a dilute solution of formalin (1%, 20  $\mu\text{L}$ /paw) into the dorsal surface of the mouse hind paw evoked biphasic nociceptive behavioral responses, such as licking, biting the injected paw, or both, occurring from 0 to 10 min after formalin injection (the early phase) and a prolonged phase, occurring from 10 to 40 min (the late phase). Before the test, mice were individually placed in a Plexiglas observation cage (30  $\times$  14  $\times$  12 cm) for one hour, to acclimatize to the testing environment. The total time the animal spent licking or biting its paw during the early and late phase of formalin-induced nociception was recorded.

### 3.8.6. Data Analysis and Statistics

Experimental *in vivo* data were expressed as mean  $\pm$  s.e.m. Significant differences among the groups were evaluated with one-way ANOVA followed by Dunnett's multiple comparisons test. GraphPad Prism 6.03 software was used for all the analyses. Statistical significance was set at  $p < 0.05$ . The data and statistical analysis comply with the recommendations on experimental design and analysis in pharmacology.

## 4. Conclusions

KORs play a crucial role in the pathogenesis of various disorders affecting the central nervous system, such as depression, anxiety, and pain. The stimulation of KOR leads to rather complex effects that reflect the structural complexity of this class of G protein coupled receptors. *In silico* experiments play an important role in the early stages of drug discovery, allowing one to reduce the time and costs associated with the identification of new molecules. In this experimental project, we used the computational technique of virtual screening to identify molecular structures that could show affinity for the KOR

through significant interactions. In this phase, the virtual library, consisting of ~6 million molecules, was submitted to the HTVS rapid docking method. Among the 33 selected molecules, the H-D-Tyr-Val-NH<sub>2</sub> dipeptide turned out to be of particular interest due to its structural requirements; therefore, it was considered for the next rational design step. In the drug design phase, we exploited knowledge about the KOR structure, designing tripeptides with higher docking score values than the JD<sub>Tic</sub> crystallographic ligand and a more marked lipophilicity, with the aim of improving the pattern of hydrophobic interactions within the orthosteric receptor site. The most promising tripeptides were further analyzed through molecular dynamics simulations, which provided a more detailed picture of the evolution of tripeptide-KOR complexes. The entire in silico process furnished the necessary data to identify and estimate the most suitable compounds for synthesis and pharmacological tests.

The two tripeptides H-D-Tyr-Val-Val-O-(3-Br)-Bz and H-D-Tyr-Val-Trp-OBz contain Tyr as the first amino acid, which is essential for the interaction with the receptor, while leaving the stereochemistry of the initial dipeptide unchanged because it showed a greater affinity for KOR. The H-D-Tyr-Val-Val-O-(3-Br)-Bz structure was found to be the most stable within the receptor's active site and recorded the highest docking score; these results are probably due to improved hydrophobic interactions involving important amino acid residues, such as Ile294, Val118, and Tyr312. The HD-Tyr-Val-Trp-OBz tripeptide does not show significant values in MD simulation analyses; however, it exhibits favorable stabilization in the receptor pocket due to additional hydrophobic interactions with Tyr139, Ile290, and Trp287, as well as a docking value score higher than JD<sub>Tic</sub>. This shows structural similarities with the endogenous opioid tetrapeptide EM-2 (H-Tyr-Pro-Trp-Phe-NH<sub>2</sub>) selective on MOR. In vivo tests revealed their ability to induce an antinociceptive effect after i.c.v. and s.c. administrations in the tail flick and formalin tests, respectively. Among them, peptide **11** is active also in the second phase of the last test. This is somewhat in agreement with the ADME prediction, which indicates a possible inhibition of the drug-metabolizing cytochrome CYP3A4 and a low GIA absorption. However both of them show poor bioavailability, prompting us to further investigate their structural modifications with the aim of improving the pharmacokinetic properties and drug-likeness. Overall this experimental work allowed us to find interesting lead compounds for the next steps of structure optimization and pharmaceutical characterization.

**Supplementary Materials:** The following are available online, Figure S1: 1H-NMR of peptide **6**; Figure S2: LRMS of peptide **5**; Figure S3: 1H-NMR of peptide **11**; Figure S4: LRMS of peptide **10**; Figure S5: ADME prediction for peptide **6**; Figure S6: ADME prediction for peptide **11**.

**Author Contributions:** Conceptualization, A.M.; Data curation, A.S. and A.D.V.; Formal analysis, V.I., G.S. and E.N.; Investigation, P.M.; Methodology, V.I.; Resources, S.P. and S.M.; Software, V.I. and S.M.; Validation, A.M.; Writing—original and draft, A.S.; Writing—review and editing, A.S., A.D.V., E.N. and A.M. All authors have read and agreed to the published version of the manuscript.

**Funding:** This research received no external funding.

**Institutional Review Board Statement:** The Service for Biotechnology and Animal Welfare of the Istituto Superiore di Sanità and the Italian Ministry of Health authorized the experimental protocol according to Legislative Decree 26/14.

**Conflicts of Interest:** The authors declare no conflict of interest.

**Sample Availability:** Samples of the compounds **6** and **11** are available from the authors.

## References

1. Brownstein, M.J. A brief History of opiates, opioid peptides, and opioid receptors. *Proc. Natl. Acad. Sci. USA* **1993**, *90*, 5391–5393. [[CrossRef](#)]
2. Williams, J.T.; Ingram, S.L.; Henderson, G.; Chavkin, C.; Von Zastrow, M.; Schulz, S.; Koch, T.; Evans, C.J.; Christie, M.J.; Dolphin, A.C. Regulation of  $\mu$ -Opioid Receptors: Desensitization, Phosphorylation, Internalization, and Tolerance. *Pharmacol. Rev.* **2013**, *65*, 223–254. [[CrossRef](#)]

3. Chavkin, C.; James, I.F.; Goldstein, A. Dynorphin is a specific endogenous ligand of the  $\kappa$  opioid receptor. *Science* **1982**, *215*, 413–415. [[CrossRef](#)] [[PubMed](#)]
4. Carlezon, W.A.; Thome, J.; Olson, V.G.; Lane-Ladd, S.B.; Brodtkin, E.S.; Hiroi, N.; Duman, R.S.; Neve, R.L.; Nestler, E.J. Regulation of Cocaine Reward by CREB. *Science* **1998**, *282*, 2272–2275. [[CrossRef](#)] [[PubMed](#)]
5. Pfeiffer, A.; Brantl, V.; Herz, A.; Emrich, H.M. Psychotomimesis mediated by kappa opiate receptors. *Science* **1986**, *233*, 774–776. [[CrossRef](#)] [[PubMed](#)]
6. Goldstein, A.; Tachibana, S.; Lowney, L.I.; Hunkapiller, M.; Hood, L. Dynorphin-(1-13), an extraordinary potent opioid peptide. *Proc. Natl. Acad. Sci. USA* **1979**, *76*, 6666–6670. [[CrossRef](#)] [[PubMed](#)]
7. Wu, H.; Wacker, D.; Mileni, M.; Katritch, V.; Han, G.W.; Vardy, E.; Liu, W.; Thompson, A.A.; Huang, X.P.; Carroll, F.I.; et al. Structure of the human kappa-opioid receptor in complex with JDTic. *Nature* **2012**, *485*, 327–332. [[CrossRef](#)] [[PubMed](#)]
8. Che, T.; Majumdar, S.; Zaidi, S.A.; Ondachi, P.; McCorvy, J.D.; Wang, S.; Mosier, P.D.; Uprety, R.; Vardy, E.; Krumm, B.E.; et al. Structure of the Nanobody-Stabilized Active State of the Kappa Opioid Receptor. *Cell* **2018**, *172*, 55–67. [[CrossRef](#)]
9. Bruchas, M.R.; Roth, B.L. New Technologies for Elucidating Opioid Receptor Function. *Trends Pharmacol. Sci.* **2016**, *37*, 279–289. [[CrossRef](#)]
10. Thomas, J.B.; Atkinson, R.N.; Rothman, R.B.; Fix, S.E.; Mascarella, S.W.; Vinson, N.A.; Dersch, C.M.; Cantrell, B.E.; Zimmerman, D.M.; Carroll, F.I. Identification of the first trans-(3R,4R)-dimethyl-4-(3-hydroxyphenyl)piperidine derivative to possess highly potent and selective opioid kappa receptor antagonist activity. *J. Med. Chem.* **2001**, *44*, 2687–2690. [[CrossRef](#)]
11. Fredriksson, R.; Lagerstrom, M.C.; Lundin, L.G.; Schiöth, H.B. The G-Protein-Coupled Receptors in the Human Genome Form Five Main Families. Phylogenetic Analysis, Paralogon Groups, and Fingerprints. *Mol. Pharmacol.* **2003**, *63*, 1256–1272. [[CrossRef](#)]
12. Bruijnzeel, A.W. Kappa-Opioid receptor signaling and brain reward function. *Brain Res. Rev.* **2009**, *62*, 127–146. [[CrossRef](#)]
13. Waldhoer, M.; Bartlett, S.E.; Whistler, J.L. Opioid receptors. *Annu. Rev. Biochem.* **2004**, *73*, 953–990. [[CrossRef](#)]
14. Urbano, M.; Guerrero, M.; Rosen, H.; Roberts, E. Antagonists of the kappa opioid receptor. *Bioorg. Med. Chem. Lett.* **2014**, *24*, 2021–2032. [[CrossRef](#)]
15. Martin, W.R.; Eades, C.G.; Thompson, J.A.; Huppler, R.E.; Gilbert, P.E. The effects of morphine- and nalorphine- like drugs in the nondependent and morphine-dependent chronic spinal dog. *J. Pharmacol. Exp. Ther.* **1976**, *197*, 517–532. [[PubMed](#)]
16. Meng, I.D.; Johansen, J.P.; Harasawa, I.; Fields, H.L. Kappa Opioids Inhibit Physiologically Identified Medullary Pain Modulating Neurons and Reduce Morphine Antinociception. *J. Neurophysiol.* **2005**, *93*, 1138–1144. [[CrossRef](#)] [[PubMed](#)]
17. Kenakin, T.; Christopoulos, A. Signalling bias in new drug discovery: Detection, quantification and therapeutic impact. *Nat Rev. Drug Discov.* **2013**, *12*, 205–216. [[CrossRef](#)]
18. Wang, S.; Wacker, D.; Levit, A.; Che, T.; Betz, R.M.; McCorvy, J.D.; Venkatakrishnan, A.J.; Huang, X.P.; Dror, R.O.; Shoichet, B.K.; et al. D4 dopamine receptor high-resolution structures enable the discovery of selective agonists. *Science* **2017**, *358*, 381–386. [[CrossRef](#)] [[PubMed](#)]
19. Di Chiara, G.; Imperato, A. Opposite effects of mu and kappa opiate agonists on dopamine release in the nucleus accumbens and in the dorsal caudate of freely moving rats. *J. Pharmacol. Exp. Ther.* **1988**, *244*, 1067–1080.
20. Narita, M.; Funada, M.; Suzuki, T. Regulations of opioid dependence by opioid receptor types. *Pharmacol. Ther.* **2001**, *89*, 1–15. [[CrossRef](#)]
21. Spanagel, R.; Herz, A.; Shippenberg, T.S. The Effects of opioid peptides on dopamine release in the nucleus accumbens: An in vivo microdialysis study. *J. Neurochem.* **1990**, *55*, 1734–1740. [[CrossRef](#)] [[PubMed](#)]
22. Dortch-Carnes, J.; Potter, D.E. Bremazocine: A  $\kappa$ -opioid agonist with potent analgesic and other pharmacologic properties. *CNS Drug Rev.* **2005**, *11*, 195–212. [[CrossRef](#)]
23. Land, B.B.; Bruchas, M.R.; Schattauer, S.; Giardino, W.J.; Aita, M.; Messinger, D.; Hnasko, T.S.; Palmiter, R.D.; Chavkin, C. Activation of the kappa opioid receptor in the dorsal raphe nucleus mediates the aversive effects of stress and reinstates drug seeking. *Proc. Natl. Acad. Sci. USA* **2009**, *106*, 19168–19173. [[CrossRef](#)] [[PubMed](#)]
24. Robles, C.F.; McMackin, M.Z.; Campi, K.L.; Doig, I.E.; Takahashi, E.Y.; Pride, M.C.; Trainor, B.C. Effects of kappa opioid receptors on conditioned place aversion and social interaction in males and females. *Behav. Brain Res.* **2014**, *262*, 84–93. [[CrossRef](#)]
25. Roth, B.L.; Baner, K.; Westkaemper, R.; Siebert, D.; Rice, K.C.; Steinberg, S.; Ernsberger, P.; Rothman, R.B. Salvinorin A: A potent naturally occurring nonnitrogenous  $\kappa$  opioid selective agonist. *Proc. Natl. Acad. Sci. USA* **2002**, *99*, 11934–11939. [[CrossRef](#)]
26. Bruchas, M.R.; Land, B.B.; Chavkin, C. The dynorphin/kappa opioid system as a modulator of stress-induced and pro-addictive behaviors. *Brain Res.* **2010**, *1314*, 44–55. [[CrossRef](#)] [[PubMed](#)]
27. Bruchas, M.R.; Macey, T.A.; Lowe, J.D.; Chavkin, C. Kappa Opioid Receptor Activation of p38 MAPK Is GRK3- and Arrestin-dependent in Neurons and Astrocytes. *J. Biol. Chem.* **2006**, *281*, 18081–18089. [[CrossRef](#)] [[PubMed](#)]
28. McLaughlin, J.P.; Xu, M.; Mackie, K.; Chavkin, C. Phosphorylation of a carboxyl-terminal serine within the kappa-opioid receptor produces desensitization and internalization. *J. Biol. Chem.* **2003**, *278*, 34631–34640. [[CrossRef](#)]
29. Bruchas, M.R.; Land, B.B.; Aita, M.; Xu, M.; Barot, S.K.; Li, S.; Chavkin, C. Stress-induced p38 mitogen-activated protein kinase activation mediates kappa opioid-dependent dysphoria. *J. Neurosci.* **2007**, *27*, 11614–11623. [[CrossRef](#)]
30. El Rawas, R.; Amaral, I.M.; Hofer, A. Is p38 MAPK Associated to Drugs of Abuse-Induced Abnormal Behaviors? *Int. J. Mol. Sci.* **2020**, *21*, 4833. [[CrossRef](#)]

31. Bruchas, M.R.; Schindler, A.G.; Shankar, H.; Messinger, D.I.; Miyatake, M.; Land, B.B.; Lemos, J.C.; Hagan, C.E.; Neumaier, J.F.; Quintana, A. Selective p38alpha MAPK deletion in serotonergic neurons produces stress resilience in models of depression and addiction. *Neuron* **2011**, *71*, 498–511. [[CrossRef](#)]
32. Pradhan, A.A.; Smith, M.L.; Kieffer, B.L.; Evans, C.J. Ligand-directed signalling within the opioid receptor family. *Br. J. Pharmacol.* **2012**, *167*, 960–969. [[CrossRef](#)]
33. Schattauer, S.S.; Miyatake, M.; Shankar, H.; Zietz, C.; Levin, J.R.; Liu-Chen, L.Y.; Gurevich, V.V.; Rieder, M.J.; Chavkin, C. Ligand directed signaling differences between rodent and human  $\kappa$ -opioid receptors. *J. Biol. Chem.* **2012**, *287*, 41595–41607. [[CrossRef](#)] [[PubMed](#)]
34. Xu, M.; Bruchas, M.R.; Ippolito, D.L.; Gendron, L.; Chavkin, C. Sciatic Nerve ligation-induced proliferation of spinal cord astrocytes is mediated by  $\kappa$  opioid activation of p38 mitogen-activated protein kinase. *J. Neurosci.* **2007**, *27*, 2570–2581. [[CrossRef](#)]
35. White, K.L.; Robinson, J.E.; Zhu, H.; DiBerto, J.F.; Polepally, P.R.; Zjawiony, J.K.; Nichols, D.E.; Malanga, C.J.; Roth, B.L. The G protein-biased kappa-opioid receptor agonist RB-64 is analgesic with a unique spectrum of activities in vivo. *J. Pharmacol. Exp. Ther.* **2015**, *352*, 98–109. [[CrossRef](#)] [[PubMed](#)]
36. White, K.L.; Scopton, A.P.; Rives, M.L.; Bikbulatov, R.V.; Polepally, P.R.; Brown, P.J.; Kenakin, T.; Javitch, J.A.; Zjawiony, J.K.; Roth, B.L. Identification of novel functionally selective kappa-opioid receptor scaffolds. *Mol. Pharmacol.* **2014**, *85*, 83–90. [[CrossRef](#)] [[PubMed](#)]
37. Yan, F.; Bikbulatov, R.V.; Mocanu, V.; Dicheva, N.; Parker, C.E.; Wetsel, W.C.; Mosier, P.D.; Westkaemper, R.B.; Allen, J.A.; Zjawiony, J.K.; et al. Structure-based design, synthesis, and biochemical and pharmacological characterization of novel Salvinorin A analogues as active state probes of the  $\kappa$ -opioid receptor. *Biochemistry* **2009**, *48*, 6898–6908. [[CrossRef](#)] [[PubMed](#)]
38. Yongye, A.B.; Pinilla, C.; Medina-Franco, J.L.; Giulianotti, M.A.; Dooley, C.T.; Appel, J.R.; Nefzi, A.; Scior, T.; Houghten, R.A.; Martinez-Mayorga, K. Integrating computational and mixture-based screening of combinatorial libraries. *J. Mol. Model.* **2011**, *17*, 1473–1482. [[CrossRef](#)]
39. Lopez-Vallejo, F.; Giulianotti, M.A.; Houghten, R.A.; Medina-Franco, J.L. Expanding the medicinally relevant chemical space with compound libraries. *Drug Discov. Today* **2012**, *17*, 718–726. [[CrossRef](#)]
40. Poli, G.; Dimmito, M.P.; Mollica, A.; Zengin, G.; Benyhe, S.; Zador, F.; Stefanucci, A. Discovery of novel  $\mu$ -opioid receptor inverse agonist from a combinatorial library of tetrapeptides through structure-based virtual screening. *Molecules* **2019**, *24*, 3872. [[CrossRef](#)]
41. Torino, D.; Mollica, A.; Pinnen, F.; Feliciani, F.; Lucente, G.; Fabrizi, G.; Portalone, G.; Davis, P.; Lai, J.; Ma, S.W.; et al. Synthesis and evaluation of new endomorphin-2 analogues containing (Z)-alpha,beta-didehydrophenylalanine (Delta(Z)Phe) residues. *J. Med. Chem.* **2010**, *53*, 4550–4554. [[CrossRef](#)] [[PubMed](#)]
42. Giordano, C.; Sansone, A.; Masi, A.; Lucente, G.; Punzi, P.; Mollica, A.; Pinnen, F.; Feliciani, F.; Cacciatore, I.; Davis, P.; et al. Synthesis and activity of endomorphin-2 and morphiceptin analogues with proline surrogates in position 2. *Eur. J. Med. Chem.* **2010**, *45*, 4594–4600. [[CrossRef](#)] [[PubMed](#)]
43. Vardy, E.; Robinson, J.E.; Li, C.; Olsen, R.H.J.; DiBerto, J.F.; Giguere, P.M.; Sassano, F.M.; Huang, X.P.; Zhu, H.; Urban, D.J. A new DREADD facilitates the multiplexed chemogenetic interrogation of behavior. *Neuron* **2015**, *86*, 936–946. [[CrossRef](#)]
44. Fenalti, G.; Giguere, P.M.; Katritch, V.; Huang, X.P.; Thompson, A.A.; Cherezov, V.; Roth, B.L.; Stevens, R.C. Molecular control of  $\delta$ -opioid receptor signalling. *Nature* **2014**, *506*, 191–196. [[CrossRef](#)] [[PubMed](#)]
45. Fenalti, G.; Zatssepin, N.A.; Betti, C.; Giguere, P.; Han, G.W.; Ishchenko, A.; Liu, W.; Guillemyn, K.; Zhang, H.; James, D. Structural basis for bifunctional peptide recognition at human  $\delta$ -opioid receptor. *Nat. Struct. Mol. Biol.* **2015**, *22*, 265–268. [[CrossRef](#)] [[PubMed](#)]
46. Stefanucci, A.; Pinnen, F.; Feliciani, F.; Cacciatore, I.; Lucente, G.; Mollica, A. Conformationally constrained histidines in the design of peptidomimetics: Strategies for the  $\chi$ -Space control. *Int. J. Mol. Sci.* **2011**, *12*, 2853–2890. [[CrossRef](#)] [[PubMed](#)]
47. Wacker, D.; Wang, S.; McCorvy, J.D.; Betz, R.M.; Venkatakrisnan, A.J.; Levit, A.; Lansu, K.; Schools, Z.L.; Che, T.; Nichols, D.E. Crystal structure of an LSD-bound human serotonin receptor. *Cell* **2017**, *168*, 377–389. [[CrossRef](#)]
48. Feliciani, F.; Pinnen, F.; Stefanucci, A.; Costante, R.; Cacciatore, I.; Lucente, G.; Mollica, A. Structure-activity relationships of biphalin analogs and their biological evaluation on opioid receptors. *Mini Rev Med Chem.* **2013**, *13*, 11–33. [[CrossRef](#)] [[PubMed](#)]
49. Johnson, T.W.; Gallego, R.A.; Edwards, M.P. Lipophilic efficiency as an important metric in drug design. *J. Med. Chem.* **2018**, *61*, 6401–6420. [[CrossRef](#)]
50. Saha, S.; Das, R.; Divyanshi, D.; Tiwari, N.; Tiwari, A.; Dalai, R.; Kumar, A.; Goswami, C. Ratio of hydrophobic-hydrophilic and positive-negative residues at lipid-water-interface influences surface expression and channel-gating of TRPV1. *BioRxiv* **2020**, *4*, 272484. [[CrossRef](#)]
51. Ferreira de Freitas, R.; Schapira, M. A systematic analysis of atomic protein–ligand interactions in the PDB. *Med. Chem. Commun.* **2017**, *8*, 1970–1981. [[CrossRef](#)] [[PubMed](#)]
52. Daina, A.; Michielin, O.; Zoete, V. SwissADME: A free web tool to evaluate pharmacokinetics, drug-likeness and medicinal chemistry friendliness of small molecules. *Sci. Rep.* **2017**, *7*, 42717. [[CrossRef](#)] [[PubMed](#)]
53. Wolking, S.; Schaeffeler, E.; Lerche, H.; Schwab, M.; Nies, A.T. Impact of genetic polymorphisms of ABCB1 (MDR1, P-glycoprotein) on drug disposition and potential clinical implications: Update of the literature. *Clin. Pharmacokinet.* **2015**, *54*, 709–735. [[CrossRef](#)]
54. Guengerich, F.P. Cytochrome P450 and chemical toxicology. *Chem. Res. Toxicol.* **2008**, *21*, 70–83. [[CrossRef](#)] [[PubMed](#)]

55. Mbarik, M.; Poirier, S.J.; Doiron, J.; Selka, A.; Barnett, D.A.; Cormier, M.; Touaibia, M.; Surette, M.E. Phenolic acid phenylester-sand their corresponding ketones: Inhibition of 5-lypoxygenases and stability in human blood and HepaRG cells. *Pharmacol. Res. Pers.* **2019**, *7*, e00524.
56. Veber, D.F.; Johnson, S.R.; Cheng, H.Y.; Smith, B.R.; Ward, K.W.; Kopple, K.D. Molecular properties that influence the oral bioavailability of drug candidates. *J. Med. Chem.* **2002**, *45*, 2615–2623. [[CrossRef](#)]
57. Irwin, J.J.; Shoichet, B.K. ZINC—a free database of commercially available compounds for virtual screening. *J. Chem. Inf. Model.* **2005**, *45*, 177–182. [[CrossRef](#)]
58. *Schrödinger Release 2017-1: LigPrep*; Schrödinger, LLC: New York, NY, USA, 2017.
59. *Schrödinger Release 2017-1: Maestro*; Schrödinger, LLC: New York, NY, USA, 2017.
60. *Schrödinger Release 2017-1: Epik*; Schrödinger, LLC: New York, NY, USA, 2017.
61. *Schrödinger Release 2017-1: Protein Preparation Wizard*; Epik; Schrödinger, LLC: New York, NY, USA, 2017.
62. *Impact*, Schrödinger, LLC, New York, NY; Prime; Schrödinger, LLC: New York, NY, USA, 2017.
63. Olsson, M.H.M.; Søndergaard, C.R.; Rostkowski, M.; Jensen, J.H. PROPKA3: Consistent treatment of internal and surface residues in empirical pKa predictions. *J. Chem. Theory Comput.* **2011**, *7*, 525–537. [[CrossRef](#)]
64. Harder, E.; Damm, W.; Maple, J.; Wu, C.; Reboul, M.; Xiang, J.Y.; Wang, L.; Lupyan, D.; Dahlgren, M.K.; Knight, J.L.; et al. OPLS3: A Force Field Providing Broad Coverage of Drug-like Small Molecules and Proteins. *J. Chem. Theory Comput.* **2016**, *12*, 281–296. [[CrossRef](#)]
65. *Schrödinger Release 2017-1: Glide*; Schrödinger, LLC: New York, NY, USA, 2017.
66. Balboni, G.; Salvadori, S.; Guerrini, R.; Bianchi, C.; Santagada, V.; Calliendo, G.; Bryant, S.D.; Lazarus, L.H. Opioid pseudopeptides containing heteroaromatic or heteroaliphatic nuclei. *Peptides* **2000**, *21*, 1663–1671. [[CrossRef](#)]
67. Zheng, Z.; Huang, X.P.; Mangano, T.J.; Zou, R.; Chen, X.; Zaidi, S.A.; Roth, B.L.; Steven, R.C.; Katritch, V. Structure-based discovery of new antagonist and biased agonist chemotypes for the kappa opioid receptor. *J. Med. Chem.* **2017**, *60*, 3070–3081. [[CrossRef](#)] [[PubMed](#)]
68. Wand, G.S.; Ney, R.L.; Baylin, S.; Eipper, B.; Mains, R.E. Characterization of a peptide alpha-amidation activity in human plasma and tissues. *Metabolism* **1985**, *34*, 1044–1052. [[CrossRef](#)]
69. *Schrödinger Release 2017-1: Desmond Molecular Dynamics System, D.E. Shaw Research, New York, NY, 2017. Maestro-Desmond Interoperability Tools*; Schrödinger, LLC: New York, NY, USA, 2017.
70. Kräutler, V.; Van Gunsteren, W.F.; Hünenberger, P.H. A fast SHAKE algorithm to solve distance constraint equations for small molecules in molecular dynamics simulations. *J. Comput. Chem.* **2001**, *22*, 501–508. [[CrossRef](#)]
71. Petersen, H.G. Accuracy and efficiency of the particle mesh Ewald method. *J. Chem. Phys.* **1995**, *103*, 3668–3679. [[CrossRef](#)]
72. Mollica, A.; Costante, R.; Stefanucci, A.; Pinnen, F.; Lucente, G.; Fidanza, S.; Pieretti, S. Antinociceptive profile of potent opioid peptide AM94, a fluorinated analogue of biphalin with non-hydrazine linker. *J. Pept. Sci.* **2013**, *19*, 233–239. [[CrossRef](#)]
73. Mollica, A.; Carotenuto, A.; Novellino, E.; Limatola, A.; Costante, R.; Pinnen, F.; Stefanucci, A.; Pieretti, S.; Borsodi, A.; Samavati, R.; et al. Novel Cyclic Biphalin Analogue with Improved Antinociceptive Properties. *ACS Med. Chem. Lett.* **2014**, *5*, 1032–1036. [[CrossRef](#)]